Coordination Chemistry Reviews 254 (2010) 254–272

Contents lists available at ScienceDirect

Coordination Chemistry Reviews

journal homepage: www.elsevier.com/locate/ccr

Review

Catalysis by rhodium complexes bearing pyridine ligands: Mechanistic aspects

Alvaro J. Pardey[a,*], Clementina Longo[b]

[a] Centro de Equilibrios en Solución, Escuela de Química, Facultad de Ciencias, Universidad Central de Venezuela, Caracas, Venezuela
[b] Centro de Investigación y Desarrollo de Radiofármacos, Facultad de Farmacia, Universidad Central de Venezuela, Caracas, Venezuela

Contents

1. Introduction 254
2. Water-gas shift reaction 255
   2.1. Homogeneous systems 255
   2.2. Immobilized systems 256
3. Carbonylation of methanol 258
4. Reduction of nitroarenes 261
   4.1. Homogeneous systems 261
   4.2. Immobilized systems 262
5. Oligomerization and hydrocarboxylation of CO/ethylene 264
6. Hydrocarbonylation of 1-hexene 265
7. Hydroesterification and hydroformylation–acetalization of 1-hexene 266
   7.1. Homogeneous systems 266
   7.2. Immobilized systems 267
8. Hydrodechlorination of dichloroethane 267
9. Carbonylation of naphtha 268
10. Hydrogenation and hydroformylation of alkenes 268
11. Catalysis by iridium complexes bearing pyridine ligands 270
12. Summary 271
   Acknowledgment 271
   Appendix A. List of abbreviations 271
   References 271

ARTICLE INFO

Article history:
Received 14 January 2009
Accepted 7 August 2009
Available online 15 August 2009

This paper is dedicated to Professor Ralph G. Pearson on the occasion of his 90th birthday.

Keywords:
Rhodium complexes
Pyridine
Catalysis
Water-gas shift reaction
Carbonylation
Hydroformylation

ABSTRACT

The present review describes several examples of the use of soluble and immobilized complexes of rhodium with pyridine ligands as catalysts. Examples include the water-gas shift reaction, the carbonylation of methanol, the reduction of nitroarenes, the hydrocarboxylation and oligomerization of CO/ethylene, the hydrocarbonylation of 1-hexene, the hydroesterification and hydroformylation–acetalization of 1-hexene, the hydrodechlorination of dichloroethane, the carbonylation of naphtha and the hydrogenation and hydroformylation of alkenes.

1. Introduction

Nitrogen containing aromatic heterocyclic ligands such as pyridines and related compounds offer the possibilities for the synthesis of transition metal complexes with application in catal-

* Corresponding author. Tel.: +58 212 481 8723; fax: +58 212 481 8723.
E-mail address: alvaro.pardey@ciens.ucv.ve (A.J. Pardey).

0010-8545/$ – see front matter © 2009 Elsevier B.V. All rights reserved.
doi:10.1016/j.ccr.2009.08.004

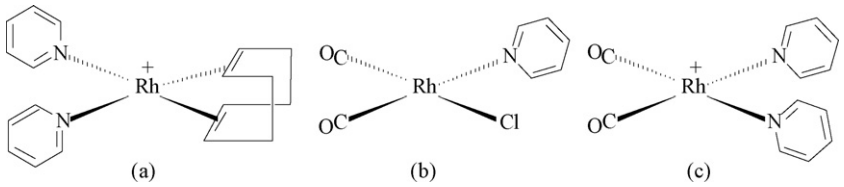

Fig. 1. Molecular models of complexes $[Rh(cod)(py)_2]^+$ (a), *cis*-$[Rh(CO)_2Cl(py)]$ (b) and *cis*-$[Rh(CO)_2(py)_2]^+$ (c) (py = pyridine).

ysis [1a,b]. N-donor ligands are classified as hard donors in the Ralph G. Pearson *hard–soft* [Lewis] acid–base (HSAB) principle [1c–g] and they can stabilize both high and low metal oxidation states. In contrast to the phosphorus atom, the N atom has no low-lying d-orbitals available and therefore N-containing ligands have only σ-donor characteristics and weak π-acceptor properties [1h]. The metal–N bond has more pronounced ionic character than the metal–P bond.

The synthesis and characterization of rhodium(I), $[Rh(cod)(amine)_2](PF_6)$, *cis*-$[Rh(CO)_2Cl(amine)]$ and *cis*-$[Rh(CO)_2(amine)_2](PF_6)$ complexes (Fig. 1; cod = 1,5-cyclooctadiene; amine = pyridine, 2-picoline, 3-picoline, 4-picoline, 3,5-lutidine or 2,6-lutidine (Fig. 2)) were reported by Denise and Pannetier [2]. These complexes are easy to prepare and to characterize and are stable in the air (with the exception of those bearing 2,6-lutidine ligand). One of the striking features of this type of complexes is the capability of being able to manipulate their electronic and steric factors by changing the position of the methyl groups present in the substituted pyridines. Such changes play an important role in their physical–chemical [3] and catalytic properties, as will be seen in the course of this review.

2. Water-gas shift reaction

The water-gas shift reaction (WGSR, Eq. (1)) is one pathway to produce pure hydrogen, also used to adjust the CO/H_2 ratios in synthesis gas, which can be further used, as an example, in the fuel cell for power generation [4]. Recent interest in this reaction has been based also on its use on elimination of carbon monoxide in the hydrogen market. Molecular hydrogen may be probably the ideal energy carrier in the foreseeable future and can be produced from water using a variety of energy sources such as solar, nuclear and fossil. Several reviews related to the homogeneous catalysis of the WGSR by transition metal complexes have been reported [5]. Professor Ralph G. Pearson also contributed with some publications related to the mechanism of water-gas shift reaction catalysis by transition metal complexes [6]:

$$CO + H_2O \rightleftarrows CO_2 + H_2 \quad (1)$$

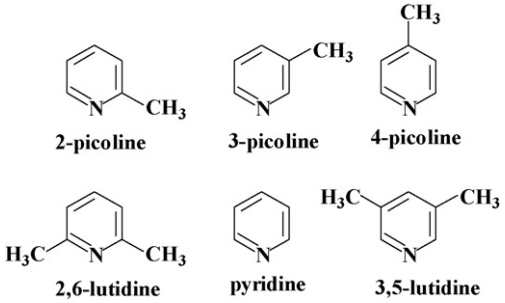

Fig. 2. Molecular models of the pyridine and substituted pyridine ligands.

2.1. Homogeneous systems

The catalysis of the WGSR by $Rh_6(CO)_{16}$ dissolved in different amines [7] and by *cis*-$[Rh(CO)_2(amine)_2](PF_6)$ (amine = pyridine, 4-picoline, or 2,6-lutidine) [8] complexes are among the first applications of the use of the Rh/amine system in such reactions. For the $Rh_6(CO)_{16}$/amine system, the $TF(H_2)$ (mole of hydrogen/mole of Rh per 24 h) follows the order 4-picoline (50) > pyridine (22) > 2-picoline (1) under 0.9 atm of CO at 100 °C. For the *cis*-$[Rh(CO)_2(amine)_2](PF_6)$/amine system, the $TF(H_2)$ (mole of hydrogen/mole of Rh per 24 h) follows the order 4-picoline (80) > pyridine (55) > 2-picoline (1) under 0.9 atm of CO at 100 °C. Steric factors, rather than electronic ones, were suggested as responsible for the low activity shown by the 2-picoline ligand for the above Rh/amine systems [8].

Extensive characterization, kinetics and mechanistic studies for the catalysis of the WGSR by $RhCl_3$/pyridine system were reported for Pardey and Ford [8] and for Fachinetti et al. [9]. The results for the *in situ* characterization studies by FT-IR and ^{13}CO NMR techniques suggest the formation of the following rhodium species *cis*-$[Rh(CO)_2(py)_2]^+$, *cis*-$[Rh(CO)(py)_3]^+$ and $[Rh_5(CO)_{13}(py)_2]-$ under the catalytic reaction conditions [8,9].

Based on the kinetics that showed the catalytic activity was first order in P(CO) and on spectroscopic studies that suggested the presence of mononuclear and polynuclear rhodium complexes. Pardey and Ford [8] proposed two mechanisms (Schemes 1 and 2) to describe the catalysis for the mononuclear species.

The authors suggested as the key step the addition of the ligand, *i.e.* CO in Scheme 1 or L in Scheme 2 (where L = a substituted pyridine). In either case the increase of the coordination number should be unfavorable for the bulky 2-substituted pyridines, for which catalytic activity is much lower.

In Scheme 1, the coordination of CO enhances the electrophilicity of all coordinated carbonyls, therefore incrementing the reactivity of these CO's toward a nucleophilic attack by H_2O. The authors stated that if this were rate limiting, then the catalysis

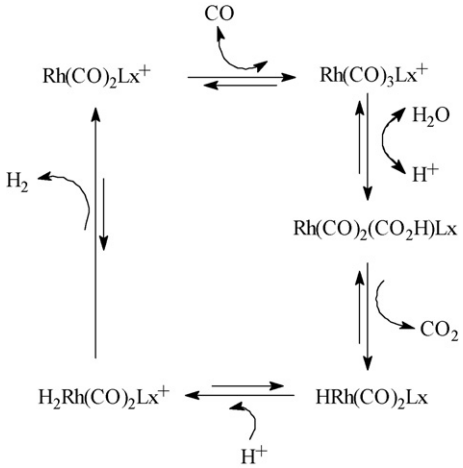

Scheme 1.

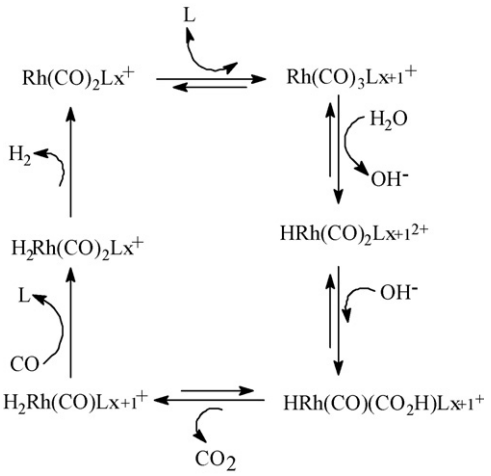

Scheme 2.

rate should be dependent on the concentration of the tricarbonyl species and therefore display a first order dependence on P(CO). The observed modest dependence of TF(H_2) on pyridine basicity is explained by the general base catalysis of the H_2O addition to the coordinated carbonyl.

In Scheme 2 the coordination of another L strongly increases the basicity of the Rh(I) center. Protonation of this $[Rh(CO)_2L_{x+1}]^+$ specie gives, the Rh(III) hydride complex, $HRh(CO)_2L_{x+1}{}^{2+}$ plus OH^- in solution. Nucleophilic attack of OH^- or H_2O on a CO coordinated gives, successively, $[HRh(CO)(CO_2H)L_{x+1}]^+$ and $[H_2Rh(CO)L_{x+1}]^+$. The equilibrium to form $[H_2Rh(CO)L_{x+1}]^+$ subsequent to the rate-limiting reductive H_2 elimination, rationalizes the first-order dependence of TF(H_2) on P(CO). Regeneration of the starting $[Rh(CO)_2L_x]^+$ complex close both catalytic cycles. In addition, the observation of a hydride signal in the NMR spectrum of the mature solution suggests that the rate-limiting step for the catalytic cycle is the H_2 elimination from the Rh(III) center.

Under catalytic conditions the observed non linear dependence of the TF(H_2) values on [Rh] implies the participation of complexes having different nuclearities in equilibrium (Fig. 3). The authors proposed analogous cycles for the polynuclear specie.

Fachinetti et al. [9a] examined the WGSR catalyzed by of $RhCl_3$ and rhodium carbonyl clusters in the presence of pyridine ligands. They were able to isolate and identify polynuclear rhodium species of the type $[(py)_2H][Rh_5(CO)_{13}(py)_2]$ formed under the catalytic conditions [9b]. The molecular structure of the anion shows that the five Rh atoms are located at the vertices of a trigonal bypyramid. There are seven terminal and six edge-bridging carbonyls. The two coordinated pyridine molecules are bonded to the Rh center located in the apical position of the trigonal bypyramidal

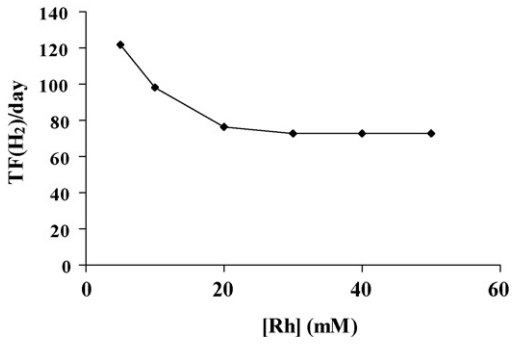

Fig. 3. Plot of TF(H_2)/day *vs.* [Rh] in 80% aqueous 4-picolina under P(CO) = 0.9 atm at 100 °C.

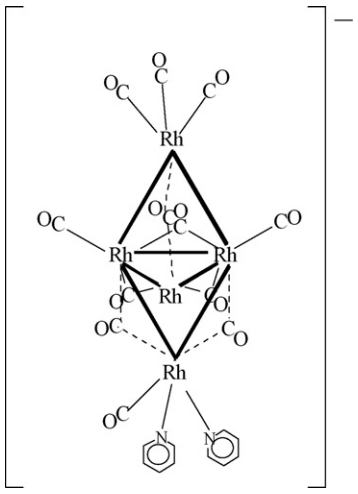

Fig. 4. Molecular structure of $[Rh_5(CO)_{13}(py)_2]^-$.

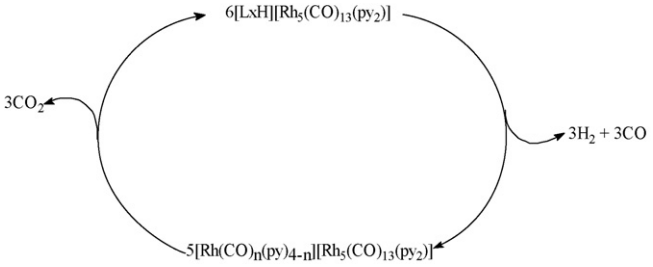

Scheme 3.

framework (Fig. 4). They proposed the mechanism described in Scheme 3.

The differences in activity noted at different rhodium concentration (Fig. 3) could be that the rate-limiting step of catalysis between these two competitive cationic mononuclear Rh and anionic polynuclear Rh complexes in equilibrium should not be the same owing to the different charges on these complexes. For example, at high concentration of Rh the equilibrium is favored toward the formation of the anionic polynuclear $[Rh_5(CO)_{13}(py)_2]^-$. As we see in Schemes 1 and 2 any nucleophilic attack by OH^- or water on the coordinated CO should not be favored due to negative charge of the anionic complex, hence decreasing the TF(H_2) values as it was observed.

The water-gas shift rates for the $RhCl_3$/aqueous pyridine are lower in comparison with the homogeneous system based on the complexes Ir(dmp-S)(cod)$^+$, where dmp-S = sulfonated derivative of 2,9-dimethyl-1,10-phenanthroline and cod = 1,5-cyclooctadiene [9c].

2.2. Immobilized systems

The immobilization of $RhCl_3$ [10a], *cis*-$[Rh(CO)_2(amine)_2](PF_6)$ [10b] and $[Rh(cod)(amine)_2](PF_6)$ [10c] in poly(4-vinylpyridine) (P(4-VP)) leads to the formation of insoluble solids which were reported to catalyze the WGSR.

Catalysis for the WGSR from $RhCl_3$ immobilized on several porous aminated polymers in contact with neutral aqueous and aqueous organic solvent media were reported by Ford et al. [10a]. Those systems using P(4-VP) as support were the most active. Values of TF(H_2) up to 12 $(24\,h)^{-1}$ were observed in aqueous 2-ethoxyethanol (80%) under P(CO) = 0.9 atm at 100 °C. Kinetics studies for these systems shows a non-linear dependence on P(CO) in the 0–1.5 atm range and a linear Arrhenius

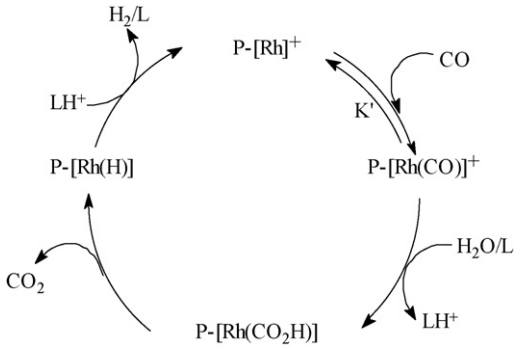

Scheme 4.

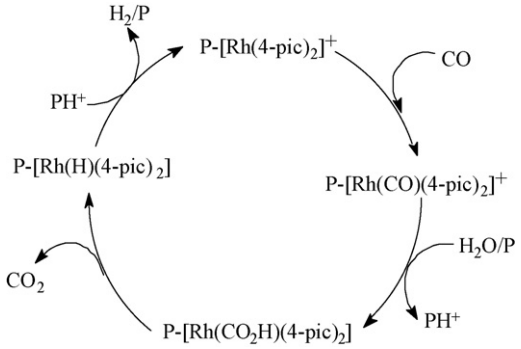

Scheme 5.

plot on the temperature range 80–110 °C with activation energy of 18 kcal/mol. A catalyst mechanism was proposed (Scheme 4, P = poly(4-vinylpyridine)).

The authors suggested that observed non linear dependence of $TF(H_2)$ on P(CO) is attributed to the reversible reaction of P–Rh^+ with CO to form the carbonyl complex P–$Rh(CO)^+$ (responsible to the observed broad ν(CO) band at 1999 cm^{-1}). The immobilized P–$Rh(CO)^+$ complex undergoes nucleophilic attack by H_2O assisted by the uncoordinated polymer pyridine, L, to give the corresponding P–$Rh(CO_2H)$ specie and the protonated polymer LH^+. Decarboxylation of P–$Rh(CO_2H)$ gives P–Rh(H) and CO_2. Protonation of P–Rh(H) by the polymer LH^+ leads to the formation of P–$Rh(H_2)$, which undergoes dihydrogen elimination to reform P–Rh^+, closing the catalytic cycle. The experimental results show that the P(4-VP) serves to immobilize the Rh catalytic species and to act as a general base and as general acid.

The water-gas shift rates of the $RhCl_3$/P(4-VP) catalytic system in contact with aqueous ethoxyethanol ($TF(H_2)$ = 12 day^{-1}) is much lower in comparison with the $RhCl_3$/aqueous pyridine system ($TF(H_2)$ = 68 day^{-1}) under similar conditions of P(CO) and temperature. This may be due the lower solubility of CO in aqueous ethoxyethanol.

Pardey et al. [10b] reported the immobilization of the complexes *cis*-$[Rh(CO)_2(amine)_2](PF_6)$ in P(4-VP) (amine = pyridine, 2-picoline, 3-picoline, 4-picoline, or 2,6-lutidine) and their ability to catalyze the WGSR under mild conditions. The results showed that $TF(H_2)$ values pursue the order: 4-picoline (8.5) > 3-picoline (7.4) > pyridine (6.9) > 2-picoline (5.7) > 2,6-lutidine (3.7) under the following reaction conditions: 0.1 g of P(4-VP), [Rh] = 8.4–9.6 (10^{-5} mol) in contact with 8 mL of 2-ethoxyethanol, 2 mL of water under P(CO) = 0.9 atm at 100 °C. The rhodium complexes bearing 4-picoline (4-pic) ligands proved to be most active among those under similar reaction conditions.

The recycling efficiency studies for the more active catalytic system $Rh(4\text{-pic})_2$/P(4-VP) shows that $TF(H_2)$ values were constant at 8.5 after three repeated runs, indicating that this polymer immobilized catalyst has a high stability and can be reused.

Spectroscopic characterization studies by FT-IR shows the replacement of the two CO of the starting *cis*-$[Rh(CO)_2(4\text{-pic})_2](PF_6)$ by the reaction with the pyridines moiety of the P(4-PV) (Eq. (2)):

$$\text{P(4-VP)} + \textit{cis}\text{-}[Rh(CO)_2(4\text{-pic})_2]^+ \rightarrow \text{P(4-VP)}\text{–}[Rh(4\text{-pic})_2]^+ + 2CO \quad (2)$$

The FT-IR spectrum of the active $Rh(4\text{-pic})_2$/P(4-VP) solid exposed to CO displays two bands at 1994 and 1833 cm^{-1} suggesting the presence of Rh linear and bridged carbonyl species on the surface of the polymer support. Also, the results of scanning electron microscopy with energy dispersive X-ray (SEM–EDX) shows the modification of the surface of the P(4-VP) after the reaction with the molecular rhodium complex bearing the 4-picoline ligand. Interesting are the EPR results reported by these authors for the $Rh(4\text{-pic})_2$/P(4-VP) before and after being exposed to CO. The fresh immobilized Rh sample shows a wide paramagnetic signal due to Rh nuclear 3/2 spin and the EPR signal intensity of the $Rh(4\text{-pic})_2$/P(4-VP) sample exposed to CO shows a decrease.

A catalyst mechanism for this $Rh(4\text{-pic})_2$/P(4-VP) system was proposed (Scheme 5, P = P(4-VP)) [10b].

In Scheme 5, carbonylation of the solid obtained from the reaction between *cis*-$[Rh(CO)_2(4\text{-pic})_2]^+$ and P(4-VP) leads to the formation of the P-$[Rh(CO)(4\text{-pic})_2]^+$. The FTIR results of the used catalyst supported the presence of Rh carbonyls complexes. Nucleophilic attack by water assisted by the general base character of the free P(4-VP) on the coordinated CO would give P-$[Rh(CO_2H)(4\text{-pic})_2]$ and the pyridinium moiety $[P(4\text{-VP})]H^+$. The decarboxylation of the former specie gives the rhodium hydride complex P-$[Rh(H)(4\text{-pic})_2]$ and protonation of the latter by $[P(4\text{-VP})]H^+$ which acts as a general acid would give H_2, free P(4-VP) and P-$[Rh(4\text{-pic})_2]^+$ to close the catalytic cycle. As in the case of the $RhCl_3$/P(4-VP) systems, the aminated polymer acts as insoluble ligand and as a general acid and base in the catalytic cycle for the $Rh(4\text{-pic})_2$/P(4-VP) system.

Pardey et al. also reported the catalysis of the WGSR by immobilized complexes formed from the reaction of $[Rh(cod)(amine)_2](PF_6)$ with P(4-VP) (cod = 1,5-cyclooctadiene, amine = pyridine, 2-picoline, 3-picoline, 4-picoline, 3,5-lutidine or 2,6-lutidine) [10c]. The $TF(H_2)$/24 h followed the order 4-picoline (11.9) > 3-picoline (9.9) > 2-picoline (5.7) > pyridine (5.4) > 3,5-lutidine (5.2) > 2,6-lutidine (3.3) under P(CO) = 0.9 atm at 100 °C in contact with 80% of aqueous 2-ethoxyethanol. The 4-picoline system displays the highest activity.

The "$Rh(4\text{-pic})_2$/P(4-VP)" systems were subject of an intensive study under flow conditions by Pardey et al. [10d]. The effect of temperature on the WGSR, catalyzed by this system, was studied at 100 ($TF(CO_2)$ = 12 day^{-1}) – 180 °C ($TF(CO_2)$ = 748 day^{-1}) range, resulting in a nonlinear Arrhenius plot with a lower activation energy E_a at temperatures below 120 °C (51 kJ/mol K) than for temperatures >120 °C (216 kJ/mol K). This segmented Arrhenius plots indicated a change in the rate-limiting step [10e].

The morphology of the immobilized catalyst was studied using a scanning electron microscope. The immobilized catalyst was also characterized by DTA–TGA analysis, FT-IR, UV–Vis reflectance, electron paramagnetic spectroscopy (EPR) and X-ray photoelectron spectroscopy (XPS), and surface area was determined by the BET method. The results were discussed in terms of the possible presence of mono- and polynuclear-immobilized rhodium species. For example, the FT-IR spectrum (in KBr) of the active Rh/4-pic immobilized catalyst exposed to CO, displays two ν(CO) bands at 1994 (carbonyl-linear Rh species) and 1832 cm^{-1} (carbonyl-bridged Rh species) suggesting the presence of rhodium carbonyl anchored

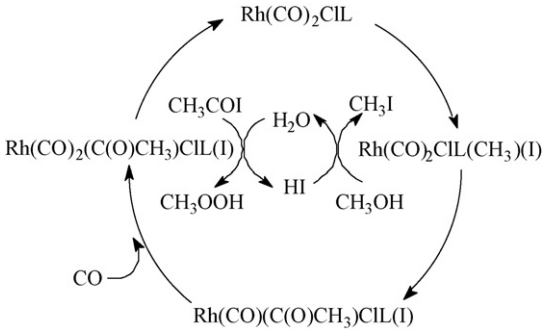

Scheme 6.

compounds with different nuclearities. The EPR and XPS studies showed the presence of Rh(II) species for fresh catalyst and XPS studies showed the presence of Rh(I) and Rh(−I) for the used catalyst.

Formation of Rh(II) is due to the air oxidation of the Rh(I) precursor $[Rh(cod)(4\text{-pic})_2](PF_6)$, which loses its stability by the replacement of the cod ligand by pyridine moieties of the P(4-VP) and leads to the formation of rhodium complexes of the type $[P(4\text{-VP})_nRh(4\text{-pic})_2]^{2+}$ as shown in Eq. (3), where the P(4-VP) acts as surface-polymer ligand as well as proton source:

$$2[Rh(cod)(4\text{-pic})_2]^+ + (1/2)O_2 + 2P(4\text{-VP})H^+ + (n-2)P(4\text{-VP})2COD + H_2O + 2[P(4\text{-VP})_nRh(4\text{-pic})_2]^{2+} \quad (3)$$

The authors based on the characterization and temperature dependence studies, suggested that the observed segmentation is the result of WGSR catalysis by both mono- and polynuclear aminocarbonyl rhodium complexes, with different energy pathways. This Rh/P(4-VP) immobilized systems has a catalytic behavior similar to the observed for the $RhCl_3$/aqueous pyridine homogeneous system. In both systems the presence of mononuclear and polynuclear carbonylrhodium complexes of pyridine ligands were confirmed spectroscopically [10d].

3. Carbonylation of methanol

Dutta and co-workers [11a] reported the carbonylation of methanol to acetic acid and its ester catalyzed by the rhodium complexes *cis*-$[Rh(CO)_2Cl(amine)]$ (amine = 2-methylpyridine, 3-methylpyridine, 4-methylpyridine, pyridine, 2-phenylpyridine, 3-phenylpyridine or 4-phenylpyridine) in presence of CH_3I under the following reaction conditions: 4 mL of methanol, 1 mL of CH_3I, 1 ml of H_2O, [Rh] = 0.054 mmol, P (CO) = 20 bar at 130 °C for 1 h and the total turnover per hour for methanol conversion to carbonylated products follows the order 3-methylpyridine (1206) > 4-methylpyridine (1087) > pyridine 4-methylpyridine (911) > 2-methylpyridine (884) > 4-phenylpyridine (840) > 3-phenylpyridine (793) > 2-phenylpyridine (735). The results show that methyl groups on the pyridines, donors of electron density to central Rh, facilitate the carbonylation due to the increase of the nucleophilicity of the Rh center. However, the electron withdrawing groups represented by the phenylpyridines slow the reaction of carbonylation. The observed lower efficiency of the "Rh(2-methylpyridine)" catalyst tested for the methylpyridine series may be due to the steric factor predominating over the electronic effect. In general, this catalytic system is more active than the well-known species $[Rh(CO)_2I_2]^-$ [11b].

A catalyst mechanism for this "Rh(amine)" system was proposed (Scheme 6, L = amine) based on the preliminary kinetics and characterization studies carried out for this group which reported that the overall rate of carbonylation depended on the rate of the oxidative addition of CH_3I to the Rh center [11a]. The IR characterization studies of the reaction mixture revealed the presence of the parent Rh(I) carbonyl complexes and the Rh(III) acyl complexes, indicating that the ligands remain bound to Rh metal center under the catalytic reaction conditions. This scheme is similar to the known mechanistic cycle for the Monsanto carbonylation of methanol process [12].

Table 1
Catalytic carbonylation of methanol by the complexes $[Rh(CO)_2ClL]$.

Ligand (L)	AcOH (%)	AcOMe (%)	Total conversion (%)	TON
Py-2-CHO	12.9	51.9	64.7	1243
Py-3-CHO	3.9	28.7	32.6	626
Py-4-CHO	6.6	35.1	41.7	801

Dutta and co-workers [11c] also reported the catalytic carbonylation of methanol to acetic acid and its ester by dicarbonylrhodium(I) complexes $[Rh(CO)_2ClL]$ of the pyridine-aldehyde ligands (L = Py-2-CHO, Py-3-CHO and Py-4-CHO) in presence of CH_3I. The results are shown in Table 1. Reaction conditions: $[CH_3OH]$ = 0.099 mol (4 cm^3), $[CH_3I]$ = 0.016 mol (1 cm^3), $[H_2O]$ = 0.054 mol (1 cm^3) and [complex] = 0.054 mmol at 130 ± 2 °C and P(CO) = 35 ± 3 bar pressure for 1 h. AcOH = acetic acid, AcOMe = methyl acetate, TON = mole of product per mole of catalyst.

The TON values follows the order Py-2-CHO > Py-4-CHO > Py-3-CHO. This trend towards carbonylation could not be explained based on the donor capability of the pyridine-aldehyde ligands because the presence of electron-withdrawing –CHO group at the 2- and 4-positions of the pyridine ring of the ligands should reduce the basicity of the N-atom and consequently tend to lower the catalytic activities. However, because the oxidative addition of CH_3I is the rate-determining step in carbonylation of methanol, the accelerating the oxidative addition reaction increases the catalytic activity. The same authors reported the kinetic study of oxidative addition reaction of CH_3I with these three complexes and they observed the follows order Py-2-CHO > Py-4-CHO > Py-3-CHO for the rate. Therefore, difference in catalytic reactivity matches the observed difference in rate for the oxidative addition reaction.

The high reactivity of complex with L = Py-2-CHO over the others two may be due to the improvement of nucleophilicity on the Rh center by the adjacent group [11d] where the substituted group on the *ortho*-position probably interacts with the Rh center by some non-conventional secondary interaction and thus effect could overcome the sterical impediment [11e].

The catalytic activity of these complexes in carbonylation of methanol, in general, is higher (TON = 801–1243) than that of the well-known species $[Rh(CO)_2I_2]^-$ (TON = 650).

In 2007, Dutta and co-workers [11f] reported carbonylation activity of methanol to acetic acid and its ester in presence of CH_3I under CO catalyzed by dicarbonylrhodium(I) complexes $[Rh(CO)_2ClL]$, with pyridine-ester ligands of the type methyl picolinate, methyl nicotinate, methyl isonicotinate, ethyl picolinate, ethyl nicotinate and ethyl isonicotinate. In addition, the kinetic study of oxidative addition of CH_3I with these complexes was also examined.

Table 2 summarizes the catalytic results for the reaction conditions: $[CH_3OH]$ = 0.099 mol (4 cm^3), $[CH_3I]$ = 0.016 mol (1 cm^3), $[H_2O]$ = 0.055 mol, (1 cm^3) and [complex] = 0.054 mmol at 130 ± 5 °C and P(CO) = 35 ± 2 bar for 1 h. AcOH = acetic acid, AcOMe = methyl acetate, TON = mole of product per mole of catalyst. Fig. 5 shows the structure of these complexes and Fig. 6 the molecular models of these ligands [11g].

Total conversion (%) values for methyl acetate formation are much greater (3.9–12.4 folds) acetic acid production. The effect of different ligands on the efficiency of catalytic carbonylation

Table 2
Catalytic carbonylation of methanol by the complexes $[Rh(CO)_2ClL]$.

Ligand (L)	AcOH (%)	AcOMe (%)	Total conversion (%)	TON
Methyl picolinate	4.50	40.00	44.50	853
Methyl nicotinate	7.55	38.31	45.86	890
Methyl isonicotinate	4.20	39.90	44.10	844
Ethyl picolinate	8.80	49.50	58.30	1117
Ethyl nicotinate	9.55	36.92	46.47	910
Ethyl isonicotinate	4.90	60.70	65.60	1251

reaction is found to follow the order ethyl isonicotinate > ethyl picolinate > ethyl nicotinate > methyl nicotinate > methyl picolinate > methyl isonicotinate. Besides, the ethyl containing ester ligands show higher catalytic activities over the methyl containing ones.

The observed tendency in activities among the complexes containing ethyl ester ligands towards catalytic carbonylation is substantiated by the observed trend in the rate of the oxidative addition reaction of CH_3I with these complexes, which shows the order isonicotinate > ethyl picolinate > ethyl nicotinate. Interesting, the difference in catalytic reactivity matches the observed difference in rate for the oxidative addition reaction. It is well known that in catalytic carbonylation of alcohol, oxidative addition reaction of alkyl halide is the rate determining step [11h]; therefore, the higher the rate of oxidative addition reaction the higher is the catalytic activity. However, the carbonylation activity of methanol did not follow the trend for the observed rate for the oxidative addition reaction of CH_3I with these complexes, which shows the order methyl picolinate > methyl isonicotinate > methyl nicotinate [11f]. Accordingly, this behavior could be explained based on the donating capabilities of the methyl ester ligands which in the presence their electron-withdrawing $–COOCH_3$ group at the *ortho*- and *para*-positions on the pyridine ring of the ligand diminishes effectively the basicity of the N-donor and consequently tends to lower the catalytic activity.

The high activity of the methyl picolinate complex compared to that of methyl isonicotinate is due to the high nucleophilicity caused by chelation through decarbonylation reaction (Fig. 7), which enhances the nucleophilicity of the Rh center. The higher rate of methyl isonicotinate over methyl nicotinate may be due to

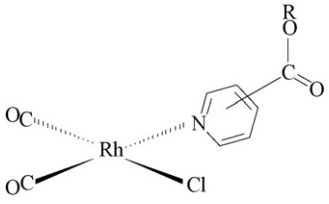

Fig. 5. Structure of complexes $[Rh(CO)_2ClL]$ (L = pyridine-ester ligands, R = $-CH_3$, or $-C_2H_5$).

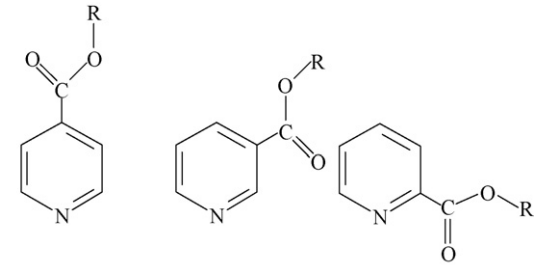

Fig. 6. Molecular models of the pyridine-ester ligands (R = methyl or ethyl).

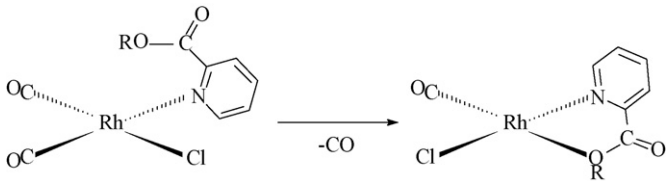

Fig. 7. Decarbonylation reaction of the picolinate complexes $[Rh(CO)_2ClL]$ (R = $-CH_3$, or $-C_2H_5$).

Table 3
Catalytic carbonylation of methanol by the complexes $[Rh(CO)_2ClL]$.

Ligand (L)	AcOH (%)	AcOMe (%)	Total conversion (%)	TON
2-Hydroxymethylpyridine	3.5	27.7	31.2	600
3-Hydroxymethylpyridine	2.5	25.7	28.2	542
4-Hydroxymethylpyridine	4.7	29.1	33.8	649

the presence of $–COOCH_3$ group at sterically less hindered *para*-position of the pyridine ring (Fig. 6).

The catalytic activity of these complexes in carbonylation of methanol, in general, is higher (TON = 844–1251) than that of the well-known species $[Rh(CO)_2I_2]^-$ (TON = 653) measured at the same reaction conditions.

In 2008, Dutta and co-workers [11i] reported carbonylation activity of methanol to acetic acid and its ester in presence of CH_3I under CO catalyzed by dicarbonylrhodium(I) complexes $[Rh(CO)_2ClL]$, with pyridine-alcohol ligands of the type 2-hydroxymethylpyridine, 3-hydroxymethylpyridine and 4-hydroxymethylpyridine. In addition, the kinetic study of oxidative addition of CH_3I with these complexes was also examined.

Table 3 summarizes the catalytic results for the reaction conditions: $[CH_3OH] = 0.099$ mol (4 cm^3), $[CH_3I] = 0.016$ mol (1 cm^3), $[H_2O] = 0.055$ mol (1 cm^3) and [complex] = 0.054 mmol at $130 \pm 5\,^{\circ}C$ under $P(CO) = 35 \pm 2$ bar for 1 h. AcOH = acetic acid, AcOMe = methyl acetate, TON = mole of product per mole of catalyst. Fig. 8 shows the molecular models of these ligands.

The effect of different pyridine-alcohol ligands on the efficiency of catalytic carbonylation reaction follows the order 4-hydroxymethylpyridine > 2-hydroxymethylpyridine > 3-hydroxymethylpyridine under the same experimental conditions The rate of the oxidative addition reaction of CH_3I with these three complexes shows the order 3-hydroxymethylpyridine > 4-hydroxymethylpyridine > 2-hydroxymethylpyridine where the complex with the 3-hydroxymethylpyridine ligand shows the highest rate for the oxidative addition reaction. Accordingly, the trend in activities by the complexes towards catalytic carbonylation reaction cannot be explained based on the observed trend on the rates of the oxidative addition of CH_3I on the Rh center.

The influence of steric factors can be used to explain this discrepancy, namely the highest catalytic activity is shown by the complex bearing the hydroxymethyl group in the least hindered 4-position of the pyridine ring. Further, the higher activity of the complex 2-hydroxymethyl over 3-hydroxymethyl may be due to the enhancement of nucleophilicity on the Rh center by some kind

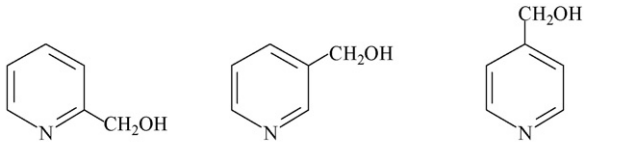

Fig. 8. Molecular models of the pyridine-alcohol ligands.

Table 4
Catalytic carbonylation of methanol by the complexes $[Rh(CO)_2L']$ and $[Rh(CO)_2ClL]$.

Complex	AcOH (%)	AcOMe (%)	Total conversion (%)	TON
(1)	6.20	41.80	48.0	923
(2a)	9.40	47.50	56.90	1094
(2b)	6.55	35.55	42.10	810

of neighboring group effect where the hydroxymethyl group in 2-position overcomes the steric hindrance probably by some non-conventional secondary interactions with the Rh centers.

The catalytic activity of these complexes with hydroxymethyl groups in carbonylation of methanol, in general, is higher (TON = 649–542) than that of the well-known species $[Rh(CO)_2I_2]^-$ (TON = 526) measured at the same reaction conditions.

More recently, in 2009, the authors reported [11j] carbonylation activity of methanol to acetic acid and its ester in presence of CH_3I under CO catalyzed by dicarbonylrhodium(I) chelates complexes $[Rh(CO)_2L']$, $\{L' = \eta^2\text{-(N,O)}\}$ with the pyridine-carboxylic acid ligand of the type Py-2-COOH (1), and the non-chelate complexes $[Rh(CO)_2ClL]$ $\{L = \eta^1\text{-(N)}\}$ with the pyridine-carboxylic acid ligands of the type Py-3-COOH (2a) and Py-4-COOH (2b). In addition, the kinetic study of oxidative addition of CH_3I with these complexes was also examined.

Table 4 summarizes the catalytic results for the reaction conditions: $[CH_3OH] = 0.099$ mol (4 cm^3), $[CH_3I] = 0.016$ mol (1 cm^3), $[H_2O] = 0.055$ mol (1 cm^3) and [complex] = 0.054 mmol at 130 ± 5 °C under $P(CO) = 30 \pm 5$ bar for 1 h. AcOH = acetic acid, AcOMe = methyl acetate, TON = mole of product per mole of catalyst. Fig. 9 shows the molecular models of these complexes.

The effect of different pyridine-carboxylic acid ligands on the efficiency of catalytic carbonylation reaction follows the order $[Rh(CO)_2Cl(Py\text{-}3\text{-}COOH)]$ (2a) > $[Rh(CO)_2(Py\text{-}2\text{-}COO^-)]$ (1) > $[Rh(CO)_2Cl(Py\text{-}4\text{-}COOH)]$ (2b). However, the catalytic conversions of methanol by these complexes are slightly lower than those reported earlier by this group [11f] where analogous alkoxycarbonyl pyridine derivatives were used. The catalytic activity of these complexes in carbonylation of methanol, in general, is higher (TON = 810–109a) than that of the well-known species $[Rh(CO)_2I_2]^-$ (TON = 653) measured at the same reaction conditions.

Examination of the catalytic reaction mixture by IR spectroscopy at different time intervals and at the end of the catalytic reaction reveals that the ligands remained coordinated to the Rh center throughout the entire course of the catalytic reactions.

The efficacy of these complexes towards the carbonylation is explained based on the electron donating capacity of the ligands. The presence of COOH group at the 2- and 4-positions of the pyridine ring in their corresponding complexes 1 and 2b should reduce the basicity of N-atom and consequently tend to lower the catalytic activity of 1 and 2b compared to the complex 2a. The higher activity of 1 over 2b may be attributed to the higher stability of the complex due to formation of five-member chelate ring (Fig. 9(1)). It is well known that the higher the nucleophilicity of the metal center the higher is the catalytic activity of the corresponding complexes towards the carbonylation of methanol.

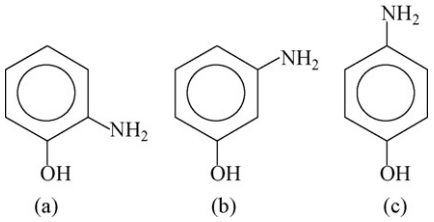

Fig. 10. Molecular models of the aminophenol ligands: 2-aminophenol (a), 3-aminophenol (b) and 4-aminophenol (c).

Table 5
Catalytic carbonylation of methanol by the complexes $[Rh(CO)_2ClL]$.

L	AcOH (%)	AcOMe (%)	Total conversion (%)	TON
2-Aminophenol	36.6	43.3	79.9	1189
3-Aminophenol	28.7	65.7	94.4	1456
4-Aminophenol	31.0	50.8	81.7	1261

A catalyst mechanism similar to earlier reported [11a] by this group was proposed (Scheme 6).

Dutta and co-workers [11k] reported carbonylation activity of methanol to acetic acid and its ester by analogues pyridine type ligands based on aminophenol (2-aminophenol (a), 3-aminophenol (b) and 4-aminophenol (c)) coordinated to dicarbonylrhodium(I) complexes, $[Rh(CO)_2ClL]$ in presence of CH_3I under CO. The IR characterization study of these complexes reveals the coordination of the aminophenol ligands through N atom of the amine group. AcOH = acetic acid, AcOMe = methyl acetate, TON = mole of product per mole of catalyst. Fig. 10 shows the molecular models of these ligands.

Table 5 summarizes the catalytic data under the best catalytic reaction conditions: $[CH_3OH] = 0.099$ mol, $[CH_3I] = 0.016$ mol, $[H_2O] = 0.055$ mol, [complex] = 0.054 mmol, substrate/catalyst = 1600; $P(CO) = 35 \pm 2$ bar at 130 ± 5 °C for 2 h.

The results show that TON values follow the order 3-aminophenol > 4-aminophenol > 2-aminophenol. However, the presence of the $(OH)^-$ group at 2- and 4-positions enhances the electron density on the N-atom which follows as 2-aminophenol > 4-aminophenol > 3-aminophenol. However, the presence of the $(OH)^-$ group at 2- and 4-positions enhances the electron density on the N-atom which follows as 2-aminophenol > 4-aminophenol > 3-aminophenol. Accordingly, the observed tendency in reactivity cannot be explained only from the simple electron donating capacity of the ligand. The authors based on the effect of steric factors, hydrogen bonding, field effects and phenoxide formation, suggested that the cumulative effect of all these factors could increase the efficiency of the catalyst with the ligand 3-aminophenol over the rest.

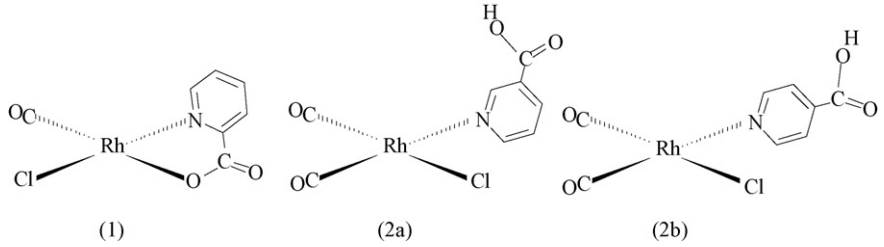

Fig. 9. Molecular models of the Rh complexes $[Rh(CO)_2L']$ and $[Rh(CO)_2ClL]$.

4. Reduction of nitroarenes

4.1. Homogeneous systems

Results of the reduction of nitrobenzene to aniline (Eq. (4)) catalyzed by the rhodium complexes *cis*-$[Rh(CO)_2(amine)_2](PF_6)$ dissolved in the corresponding aqueous amine ligand under CO atmosphere were described by Linares et al. [13a]. The TF(aniline)/24 h values pursue the order: 2-picoline (42) > 2,6-lutidine (37) > 3-picoline (28) > 4-picoline (10) > pyridine (7) for the following reaction conditions: [Rh] = 10 mM, S/C = 2500, 8 mL of amine, 2 mL of water, P(CO) = 0.9 atm at 100 °C for 3 h, with a selectivity towards aniline formation greater than 99%:

$$C_6H_5NO_2 + 3CO + H_2O \rightarrow C_6H_5NH_2 + 3CO_2 \quad (4)$$

The results show that, contrary to the water-gas shift rates, the most active catalysts for the reduction of nitrobenzene to aniline under water-gas shift conditions were those containing the sterically hindered 2-picoline and 2,6-lutidine.

Studies carried out by Longo et al. on the activity of the more active "$Rh(2\text{-picoline})_2$" catalyst in the reduction of nitrobenzene to aniline, allowed those workers to propose a mechanism [13b]. The reaction showed a first order dependence with respect to variation of the pressure of CO in the range of 0–1.9 atm. This kinetic behavior was interpreted as the CO addition to catalytic species before the determining step. Moreover, the dependence of the catalytic activity was not linear with respect to the [Rh] in the range of 5–60 mM, just as it is with respect to variation in temperature in the range of 70–130 °C. These observations were interpreted in terms of the presence of rhodium catalytic species with different nuclearity and catalytic behavior, which is reinforced by studies of *in situ* IR characterization of the catalytic solution that revealed the presence of species of ligands with Rh carbonyls terminals and bridged. A catalyst mechanism for this "$Rh(2\text{-picoline})_2$" system was proposed (Scheme 7, 2-pic = 2-picoline; RNO_2 = nitrobenzene).

In Scheme 7, the cycloaddition of the nitro group (step 1a) to the Rh–CO bond gives $[Rh(CO)(2\text{-pic})_2(\eta^2\text{-C(O)ON(R)O)}]^+$, Ragaini et al. isolated and characterized by X-ray crystallography the $PPN[(CO)_2Rh(\eta^2\text{-C(O)ON}(C_6H_3Cl_2)O)]$ intermediate [14a] (Fig. 11). Elimination of CO_2 from $[Rh(CO)(2\text{-pic})_2(\eta^2\text{-}$

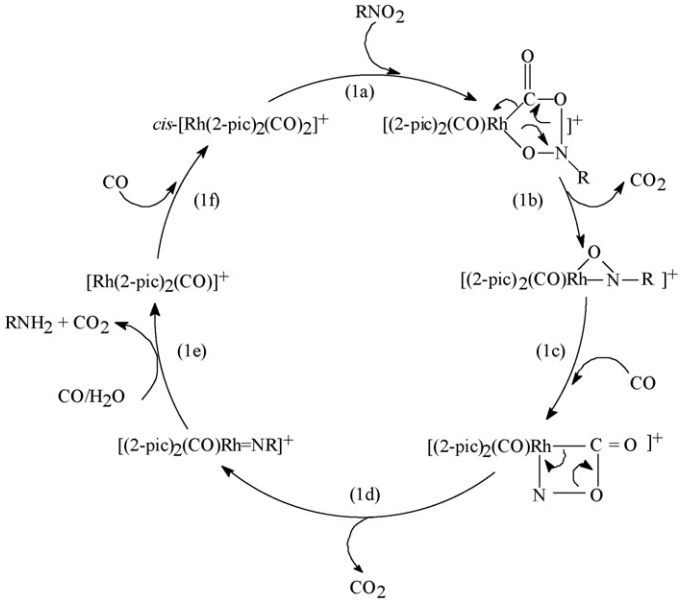

Scheme 7. Figure was reproduced from Ref. [13b], with permission of the copyright holders.

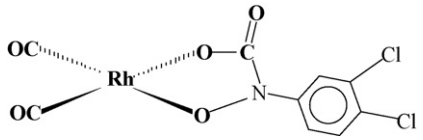

Fig. 11. Molecular model of the $[(CO)_2Rh(\eta^2\text{-C(O)ON}(C_6H_3Cl_2)O)]^-$ anion.

$C(O)ON(R)O)]^+$ intermediates (step 1b) leads to the formation of rhodium nitrosobenzene complex $[Rh(CO)(2\text{-pic})_2(\eta^2\text{-ONR})]^+$. Insertion of one CO molecule to the Rh–O bond (step 1c) forms the $[Rh(CO)(2\text{-pic})_2(\eta^2\text{-O(CO)NR})]^+$ complex. The formation of these species as the rate-limiting step would rationalize the first-order dependence of TF(aniline) on P(CO). There is also a precedent for the structures proposed; Skoog et al. isolated and characterized by X-ray crystallography the $[Ru(dppe)(CO)_2(\eta^2\text{-ONC}_6H_3ClCF_3)]$ intermediate [14b,c] (dppe = 1,2-bis(diphenylphosphino)ethane) (Fig. 12). Decarboxylation of the rhodium $[Rh(CO)(2\text{-pic})_2(\eta^2\text{-}$ $O(CO)\text{-NR})]^+$ species (step d) generates a rhodium–nitrene complex $[Rh(CO)(2\text{-pic})_2(NR)]^+$ and CO_2. Hydrogenation of this rhodium–nitrene species, probably by the Rh–H species formed under conditions similar to the WGSR (step 1e), affords aniline, CO_2 and the coordinatively unsaturated $[Rh(CO)(2\text{-pic})_2]^+$ complex. Coordination of CO to the latter (step 1f) would give the *cis*-$[Rh(CO)_2(2\text{-pic})_2]^+$ complex to close the catalytic cycle.

Ford and co-workers [15] described the quantitative studies of the CO/H_2O reduction of nitrobenzene and various *p*-nitroaromatics (*p*-X-$PhNO_2$, for X = NH_2, CH_3, H^-, F^-, Cl^- and NC–) to the respective anilines under water-gas shift reaction (WGSR) conditions catalyzed by solutions of $RhCl_3$ in aqueous amines (diethylamine, trimethylamine, triethylamine, tetramethylenediamine, 2-picoline, N,N,N′,N′-tetramethylethylenediamine (TMEDA). The reactions were carried out under the following conditions: 8/2 (v/v) amine/H_2O, $RhCl_3$ = 5 mM, [substrate] = 250 mM, P(CO) = 0.9 atm, T = 100 °C, reaction time = 3 h. They reported that the amine influence on TF(*p*-CH_3PhNH_2)/day follows the order: trimethylamine (13) > diethylamine (17) > tetramethylenediamine (20) > triethylamine (31) > 2-picoline (78) > TMEDA (131). Accordingly, the most active media were aqueous TMEDA and 2-picoline solutions.

The same authors also studied the electronic effects of phenyl ring substituents X on the series *p*-X-$PhNO_2$. The TF(aniline)/day values decreased as the substituents X become more electron withdrawing, for example, NH_2 (104) > CH_3 (102) > H (73) > F (67) > Cl (62) > NC (48) and the Hammett plot of log(TF(aniline)) versus the substituent constant σ was linear giving a ρ-value of −0.28. The rates for reduction of *p*-nitrotoluene in 80% aq. TMEDA or in 80% aq. 2-picoline exhibited first-order dependence on P(CO) over the 0.3–1.5 atm range, but turnover frequencies decreased as the total rhodium concentration increased over the range 5–40 mM. The latter behavior was interpreted in terms of the coexistence of mononuclear and polynuclear Rh species in the system, the mononuclear being the more catalytically active. Additionally, at low [substrate], H_2 production was also found as the

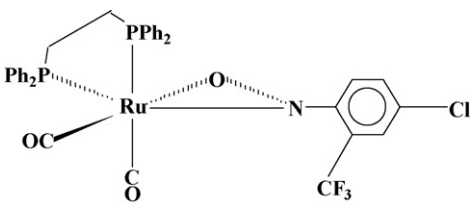

Fig. 12. Molecular model of the $[Ru(dppe)(CO)_2(\eta^2\text{-ONC}_6H_3ClCF_3)]$ complex.

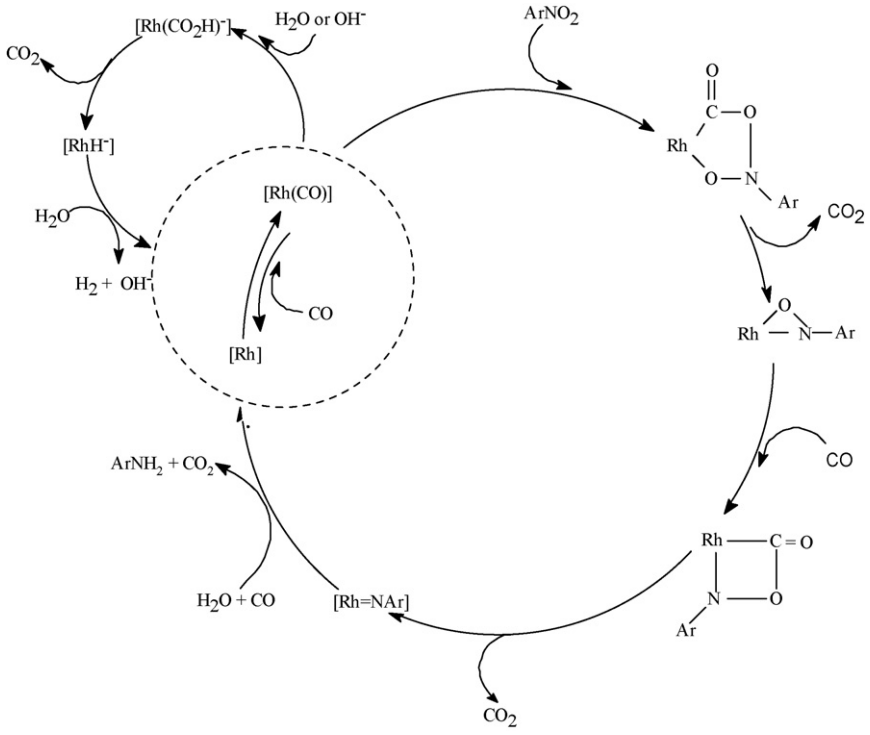

Scheme 8.

result of competing water–gas shift catalysis. TF(H_2) decreased and TF(CO_2) increased with rising [*p*-nitrotoluene], and little dihydrogen production was seen for substrate concentrations greater than 150 mM and CO_2 production leveled off in this region. The authors proposed a catalyst mechanism (Scheme 8) similar to the above reported by Longo et al. for the "Rh(2-picoline)$_2$" catalyst in the reduction of nitrobenzene to aniline under CO/H_2O. However, they incorporated the WGSR catalysis path in equilibrium with the nitroaromatic reduction catalytic cycle.

Baricelli and co-workers [16a] reported that rhodium(I) complexes of the type, *cis*-[Rh(CO)$_2$(amine)$_2$](PF$_6$) (where amine = 3-picoline, 2-picoline, pyridine, 2,6-lutidina or 3,5-lutidine) dissolved in 80% aqueous amine solutions catalyzed the selective reduction of 4-nitrobenzoic acid to 4-aminobenzoic acid under CO. The importance of these catalytic systems is their high chemo selectivity for the aromatic nitro group of the 4-nitrobenzoic acid with respect to the carboxylic group, allowing the production of the desired aromatic amine in high yields. The toxicology and carcinogenesis studies of 4-nitrobenzoic acid evidence the carcinogenic activity and hematological toxicity this acid in rats and mice [16b] and for this reasons there is an interest to transform this compound to 4-aminobenzoic acid, which is a non-toxic and does not show any carcinogenic activity.

These authors observed that 4-aminobenzoic acid production depends on the nature of the coordinated amine. The Rh/3,5-lutidine system, the most active catalyst among tested, displays turnover frequencies for 4-aminobenzoic acid production of about 173 mol/mol Rh per day for [Rh] = 1×10^{-4} mol, [4-nitrobenzoic acid] = 3.82×10^{-3} mol, 10 mL of 80% aqueous 3,5-lutidine, P(CO) = 0.9 atm at 100 °C. Analyses of kinetic results for the Rh/3,5-lutidine system show a first order dependence on 4-nitrobenzoic acid concentration, a non-linear dependence on CO pressure, and a segmented Arrhenius plot. These data were discussed in terms of mechanisms similar to described above for the reduction of nitrobenzene [13] and nitroarenes [15] under CO/H_2O.

4.2. Immobilized systems

Pardey et al. [17a] also reported results for nitrobenzene reduction catalyzed by the Rh complexes, [Rh(cod)(amine)$_2$](PF$_6$) immobilized on P(4-VP), where cod = 1,5-cyclooctadiene, immobilized on P(4-VP). The results showed that TF(aniline)/day values pursue the order: 2-picoline (53) > 4-picoline = pyridine (49) > 3-picoline (47) > 3,5-lutidine (31) > 2,6-lutidine (28) under the following reaction conditions: [Rh] = 10 mM, 8 mL of 2-ethoxyethanol, 2 mL of water, P(CO) = 0.9 atm at 100 °C for 3 h, with a selectivity towards aniline formation greater than 99%.

Contrary to the observed water-gas shift rates for the Rh/P(4-VP) [10b], the most active catalysts for the reduction of nitrobenzene to aniline under water-gas shift conditions was the sterically hindered 2-picoline ligand. The recycling efficiency of the more active Rh(2-pic)/P(4-VP) system shows no significant change of catalytic activity after three repetitive uses. The TF(aniline) values were 53, 52 and 51 day^{-1}. This solid catalyst has a high stability.

The characterization of the immobilized catalyst was also reported by the same authors using thermogravimetric analysis, infrared spectroscopy, UV–Vis, electron paramagnetic spectroscopy, and X-ray photoelectron spectroscopy. The FT-IR spectrum of a solid sample of [Rh(cod)(2-pic)$_2$](PF$_6$) shows ν(CN) bands at 1607(s), 1481(s), 1449(m) and 1435(m) cm^{-1}, and the FT-R spectrum of a solid sample of the P(4-VP) polymer shows ν(CN) bands at 1597(vs, broad), 1556(m), 1494(m), 1447(m) and 1414(vs, broad) cm^{-1}. The FT-IR spectrum of the immobilized fresh catalyst Rh(2-pic)$_2$/P(4-VP) shows ν(CN) bands at 1612(shoulder), 1599(s, broad), 1555(m), 1494(m), 1447(m) and 1418(s, broad) cm^{-1}. The FT-IR spectrum obtained from the subtraction of the FT-IR spectrum of the immobilized fresh catalyst Rh(2-pic)$_2$/P(4-VP) and the FT-IR spectrum of the P(4-VP) sample shows only two ν(CN) bands at 1612(s) and 1430(s, broad) cm^{-1}, which correspond to the ν(CN) bands of the 2-picoline ligand, coordinated to the rhodium center in the [Rh(cod)(2-pic)$_2$]$^+$ complex and they are shifted *ca.* ±5 cm^{-1} after the immobilization in the P(4-VP) polymer. The slight

blue shift observed in the ν(CN) of Rh(2-pic)$_2$/P(4-VP) indicate N-coordination of the P(4-VP) polymer to a metal center [17b–d].

The FT-IR spectrum (KBr pellets) of an active Rh(2-pic)$_2$/P(4-VP) catalyst sample displays three bands in the ν(CO) region, two at 1989 and 1961 cm^{-1} (carbonyl-linear Rh species), and one band at 1805 cm^{-1} (carbonyl-bridged Rh species). These data suggested the presence of carbonylrhodium compounds, immobilized to the nitrogen-functionalized polymer as reaction intermediates.

The EPR spectrum of [Rh(cod)(2-pic)$_2$](PF$_6$) shows no paramagnetic signal, as was expected for this diamagnetic Rh(I) (d^8) compounds The EPR spectrum of a freshly prepared sample of Rh(2-pic)$_2$/P(4-VP) solid displayed a paramagnetic signal due to Rh(II) species (d^7)). Presumably these were formed by the oxidation of the Rh(I) precursor dissolved in aqueous ethoxyethanol solution in contact with air during the preparation step. The EPR signal intensity of Rh(2-pic)$_2$/P(4-VP) sample exposed to CO/H$_2$O markedly decreases, probably due to the reduction to non-paramagnetic rhodium species by the CO/H$_2$O couple.

By X-ray photoelectron spectroscopy, the Rh 3d$_{5/2}$ level binding energy value of [Rh(cod)(2-pic)$_2$](PF$_6$) sample was found to be 308.0 eV. The treatment of this Rh(I) complex with P(4-VP) in contact with 2-ethoxyethanol on air caused a 0.4 eV increase in the Rh 3d$_{5/2}$ level binding energy, due to the formation of Rh(II) [17e]. The spectrum of the sample of Rh(2-pic)$_2$/P(4-VP) after being used as a catalyst for the WGSR showed two Rh 3d$_{5/2}$ level binding energy values at 308.2 and 307.0 eV. The Rh 3d$_{5/2}$ level binding energy value at 308.2 eV is close to that of the precursor Rh(I). On the other hand, Rh 3d$_{5/2}$ level binding energy at 307.0 eV indicates the presence of Rh species with (0) or (−1) oxidation state. The Rh(−I)/P(4-VP) immobilized specie is formed by disproportionation reaction of Rh(0) amino-carbonyl species by the CO/H$_2$O mixture [9b].

The characterization results showed that the Rh ions are covalently attached to the nitrogen-functionalized polymer. XPS indicated that several Rh oxidation states coexist on the surface of the catalyst, which was suggested to be due to the presence of both mononuclear and polynuclear immobilized Rh species on the surface.

Pardey and co-workers [17f] also reported results for nitrobenzene reduction to azoxybenzene (Eq. (5)) catalyzed by the tetracarbonyldi-μ-chlorodirhodium(I) complex (Rh$_2$(CO)$_4$Cl$_2$) immobilized on P(4-VP) in contact with 80% aqueous 2-ethoxyethanol under CO:

$$2C_6H_5\text{–}NO_2 + 3CO \rightarrow C_6H_5\text{–}N(O) = N\text{–}C_6H_5 + 3CO_2 \quad (5)$$

Table 6 summarizes the catalytic data for the reaction conditions: 0.5 g of P(4-VP), 0.26 ml of nitrobenzene, 8 ml of 2-ethoxyethanol, 2 ml of H$_2$O, [Rh] = 2.0 wt.%, S/C molar ratio = 25, P(CO) = 0.9 atm at 100 °C for 3 h. 99% of azoxybenzene selectivity with 23% of conversion. TF = [mol of product (mol of Rh × rt)$^{-1}$] × 24 h, where rt = reaction time.

In addition, 2.07 × 10^{-3} mol of azoxybenzene (TF = 167 (24 h)$^{-1}$) were formed (selectivity > 99% with 80% of nitrobenzene conversion) after a continuous heating for 8 h under the same experimental conditions described above.

Segmented Arrhenius plots with inflection points at 90 °C were observed for catalytic reduction of nitrobenzene in the 70–110 °C ranges. The apparent activation energies obtained from the slopes of the respective segments are 75.9 kJ mol^{-1} at T < 90 °C and 30.9 kJ mol^{-1} at T > 90 °C.

Table 6
Nitrobenzene reduction by Rh$_2$(CO)$_4$Cl$_2$ immobilized on P(4-VP).

Run	TF(CO$_2$)	TF (azoxybenzene)
1	137	46
2	135	45
3	147	49

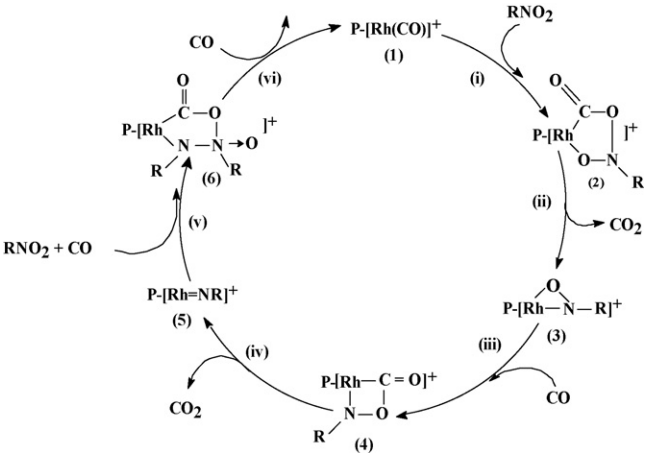

Scheme 9.

The recycling efficiency of the Rh$_2$(CO)$_4$Cl$_2$/P(4-VP) catalyst was studied in the reduction of nitrobenzene and the results showed no change of the catalytic activity after three repetitive uses (TF = 48, 47 and 49 (24)$^{-1}$). These results show the high stability of this catalytic system.

The authors carried out a detail characterization studies of the fresh and used catalyst and they reported that the FT-IR spectra of fresh prepared KBr pellets of Rh$_2$(CO)$_4$Cl$_2$/P(4-VP) ([Rh] = 2.0 wt.%) showed a broad strong ν(CO) band at 2101 cm^{-1}, contrary to the observed four bands ν(CO) at 2101, 2082, 2036 and 2022 cm^{-1} for the precursor Rh$_2$(CO)$_4$Cl$_2$ complex Interesting, the presence of the only carbonyl at band at 2101 cm^{-1} ruled out the formation of *cis*-Rh(CO)$_2$Cl-P(4-VP) species bound to a pyridine moiety of the polymer. Such species should have two ν(CO) bands at about 2100–2080 and 2040–2010 cm^{-1} [17g,h]. Formation of the *cis*-[Rh(CO)$_2$Clpy] complex by reaction of Rh$_2$(CO)$_4$Cl$_2$ with pyridine (py) is a well known process [17h]. Furthermore, the electron paramagnetic resonance spectrum of fresh samples of Rh$_2$(CO)$_4$Cl$_2$/P(4-VP) shows a paramagnetic signal indicating the formation of Rh(II) species. The authors based on the above data suggested the presence of monocarbonyl cationic Rh(II) (Rh(II)-CO/P(4-VP)) species formed during the immobilization of Rh$_2$(CO)$_4$Cl$_2$ with P(4-VP).

On the other hand, the FT-IR spectrum (KBr pellets) of an used Rh/P(4-VP) catalyst sample shows three bands in the ν(CO) region at 2101, 1955 (carbonyl-linear Rh species) and 1802 cm^{-1} (carbonyl-bridged Rh species) suggesting the presence of mononuclear and polynuclear amino-carbonyl Rh immobilized complexes as the principal catalytic species on the used catalyst. Furthermore, the EPR of the fresh Rh(II)–CO/P(4-VP) sample exposed to CO in contact with aqueous ethoxyethanol shows a complete disappearance of the paramagnetic signal attributed to reduction of the Rh(II) center to Rh(−I) and/or Rh(I) by the couple CO/H$_2$O. It can see that this catalytic system behaves in a similar way to the Rh(amine)$_2$/P(4-VP) systems [10d,17a] described in previous sections.

The authors proposed a catalyst mechanism (Scheme 9). In this scheme some ligands of the immobilized rhodium complex are omitted for clarity. Also the WGSR catalytic cycle seen in Scheme 8 is omitted. The cycloaddition of the nitro group to the Rh-CO bond (step i) forms the complex (2). Elimination of CO$_2$ from complex (2) (step ii) leads to the formation of the rhodium nitrosobenzene P-[Rh(η^2-ONR)]$^+$ complex (3) [14]. Insertion of one CO molecule to the Rh–O bond in complex (3) (step iii) form the P-[Rh(η^2-CO(O)NR)]$^+$ (4) specie. Decarboxylation

of the rhodium P-[Rh(η^2-CO(O)NR)]$^+$ (4) specie generates the rhodium–nitrene complex P-[Rh=NR]$^+$ (5) and CO_2 (step iv). Subsequent coordination of CO and cycloaddition of a second molecule of nitrobenzene (step v) to the rhodium–nitrene specie forms the P-[Rh(η^2-CO(O)N(O)RNR)]$^+$ (6) complex. In step (vi), coordination of CO to the latter complex (6) affords CO_2, azoxybenzene and P-[Rh(CO)]$^+$ (1) closing the catalytic cycle.

In the absence of nitrobenzene, this $Rh_2(CO)_4Cl_2$/P(4-VP) system catalyzed the WGSR under the following reaction conditions: [Rh] = 2 wt.%, 10 mL of water, under P(CO) = 0.9 atm at 100 °C for 4 h. The TF(H_2) and TF(CO_2) observed values were 26 and 28 day^{-1}, respectively. This systems is more active than the previously described $RhCl_3$/P(4-VP) [10a] and Rh(4-pic)$_2$/P(4-VP) [10b] WGSR catalytic systems under the same catalytic conditions.

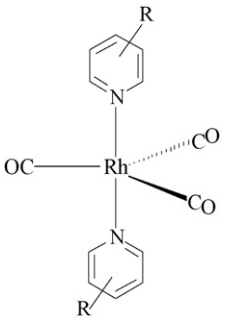

Fig. 13. Molecular model of the *trans*-[Rh(CO)$_3$(amine)$_2$]$^+$ cation (R = methyl or dimethyl group).

5. Oligomerization and hydrocarboxylation of CO/ethylene

Fachinetti and co-workers [18] reported the catalysis of the hydrocarboxylation of ethylene (Eq. (6)) and the stepwise alternating oligomerization of CO/ethylene (Eq. (7)) by the rhodium complexes *cis*-[Rh(CO)$_2$(amine)$_2$](PF$_6$) (amine = pyridine, 2-picoline, 3-picoline, 4-picoline, or 2,6-lutidine) dissolved in aqueous tetrabutyl ammonium hydrogen sulfate ([(CH$_3$(CH$_2$)$_3$)$_4$N](HSO$_4$)) solutions. Propionic acid, penta-3-one, octane-3,6-dione and undecane3,6,9-trione were obtained as major products for the catalytic reaction under the following reaction conditions: [Rh] = 1.5 × 10^{-5} mol [[(CH$_3$(CH$_2$)$_3$)$_4$N](HSO$_4$)] = 2.52 g, [H$_2$O] = 40 g, [CO] = [ethylene] = 20.0 g (88 atm) at 150 °C for 6.3 h. The use of the saline medium helps to stabilize the active species. The *in situ* IR studies of the catalytic solutions suggest the presence of penta-coordinated Rh complexes of the type *trans*-[Rh(CO)$_3$(amine)$_2$]$^+$:

$$C_2H_4 + CO + H_2O \rightarrow C_2H_5COOH \quad (6)$$

$$n(CH_2{=}CH_2) + nCO + \rightarrow H(-CH_2CH_2CO-)_nCH_2CH_3 \quad (7)$$

Reactivity towards the formation of propionic acid by this system Rh/amine depends on the nature of the amine coordinated at the center of rhodium. For example the values of TF(propionic acid) for these complexes varies in the following order: 4-picoline (558) > 3-picoline (356) = pyridine (356) > 2-picoline (330) > 2,6-lutidine (152 (24 h)$^{-1}$) under the same catalytic conditions. Additionally, the catalytic activity of the reaction of oligomerization (Eq. (8)) varies in the following order: 4-picoline (1473) > 3-picoline (1356) > 2-picoline (1252) > pyridine (1211) > 2,6-lutidine (305) under the same conditions catalytic:

$$n(CH_2{=}CH_2) + nCO + H_2O \rightarrow CH_3{-}CH_2{-}C(O){-}R + CO_2 \quad (8)$$

For $n = 2$, R = CH$_2$–CH$_3$; penta-3-one, for $n = 3$, R = CH$_2$–CH$_2$–C(O)–CH$_2$–CH$_3$; octane-3,6-dione and for $n = 4$, R = CH$_2$–CH$_2$–C(O)–CH$_2$–CH$_2$–C(O)–CH$_2$–CH$_3$; undecane3,6,9-trione.

Apparently, the catalytic activities observed for both types of reactions are a result of a fine balance between the electronic and steric properties of the amine ligand. Scheme 9 shows the catalytic cycles of these two reactions. The authors reported the reaction of the catalytic precursors *cis*-[Rh(CO)$_2$(amine)$_2$]$^+$ with CO to form the tricarbonyl-rhodium *trans*-[Rh(CO)$_3$(amine)$_2$]$^+$ com-

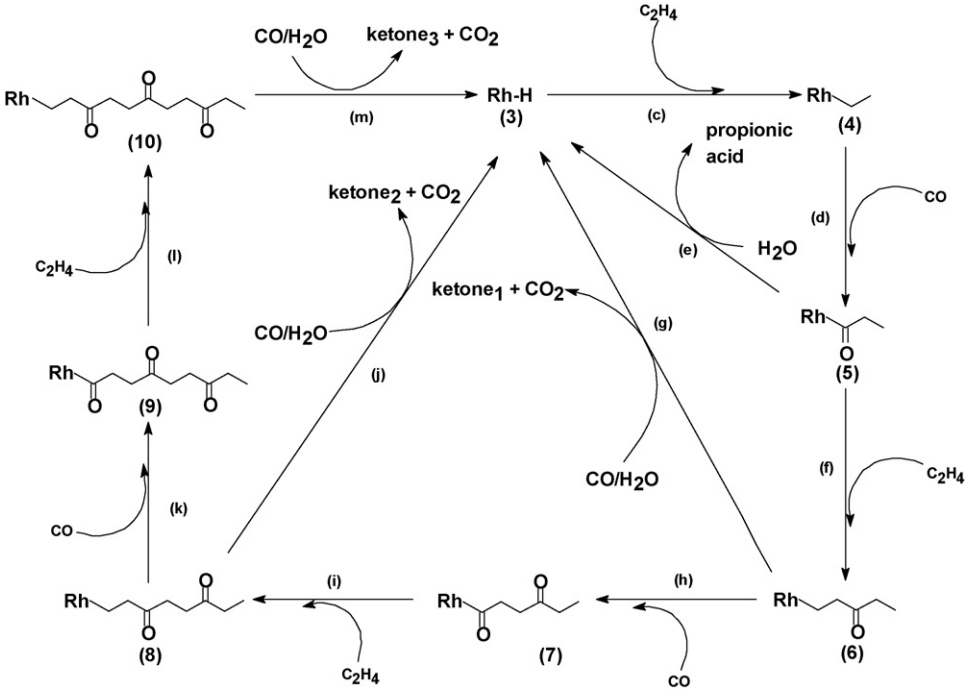

Scheme 10. Ketone$_1$ = penta-3-one; ketone$_2$ = octane-3,6-dione; ketone$_3$ = undecane-3,6,9-trione. Figure was reproduced from Ref. [18], with permission of the copyright holders.

plex (Eq. (9), Fig. 13), which under CO/H_2O is gradually transformed in the neutral complex $[HRh(CO)_2(amine)_2]$ (Eq. (10)); the "Rh–H" in Scheme 9. The characterization by *in situ* ^1H NMR spectroscopic studies of rhodium hydride intermediates (Rh–H) formed by the transformation of the rhodium(I) complex, *cis*-$[Rh(CO)_2(py)_2](PF_6)$ dissolved in aqueous pyridine was previously reported [8]:

$$cis\text{-}[Rh(CO)_2(amine)_2]^+ + CO \rightarrow trans\text{-}[Rh(CO)_3(amine)_2]^+ \quad (9)$$

$$trans\text{-}[Rh(CO)_3(amine)_2]^+ + H_2O \rightarrow [HRh(CO)_2(amine)_2] + H^+ + CO_2 \quad (10)$$

In Scheme 10, the CO and the amine ligands of the starting rhodium complex (3) are omitted for clarity. The authors proposed that propionic acid formation (step e) and ketones (steps g, j and m) arise by hydrolysis and hydrogenolysis, of the Rh-acyl intermediates, respectively and that oligomerization proceeded by a single mode of chain growth involving alternate insertion of CO and ethylene (C_2H_4) forming intermediate Rh-acyls, where Rh-acyl species react with the CO/H_2O couple affording CO_2 and the corresponding ketones.

It seems that the role of the coordinated pyridine is to facilitate the formation of propionic acid. It has been proposed that pyridine has vacant antibonding π-orbitals, capable of accepting the electrons coming from rhodium-back donation, lowering the electron density on the Rh center [19]. Accordingly, the pyridine coordinated σ-acyl complex (5) may be easily attacked by nucleophilic OH^- groups (coming from H_2O) giving propionic acid (step e). The hydrogenolysis of the Rh-acyl intermediates, which leads to ketone formation (steps g, j and m), comes probably from *intra*-hydrogen transfer from Rh–H species formed under conditions similar to the WGSR [8].

6. Hydrocarbonylation of 1-hexene

Hung-Low et al. [20a] described the hydrocarbonylation of 1-hexene to heptanoic acid catalyzed by rhodium(I) $[Rh(cod)(amine)_2](PF_6)$ complexes (cod = 1,5-cyclooctadiene; amine = pyridine, 2-picoline, 3-picoline, 4-picoline, 3,5-lutidine or 2,6-lutidine) immobilized on P(4-VP) in contact with water under carbon monoxide atmosphere. Gaseous by-products H_2 and CO_2 coming from the catalysis of WGSR were also observed. Table 7 summarizes the water-gas shift and hydrocarbonylation of 1-hexene rate data for the Rh catalysts with different pyridine and substituted pyridine ligands for the conditions: 0.5 g of P(4-VP), [Rh] = 2.0 wt.% (1×10^{-4} mol), 10 mL of H_2O, 1.24 mL of 1-hexene (1×10^{-2} mol), 1-hexene/Rh = 100, P(CO) = 0.9 atm at 100 °C for 5 h. TF(product) = [(mol of product)/(mol of Rh) × (rt)] × 24 h, where (rt) = reaction time in hours.

The rate data related to the hydroxycarbonylation of 1-hexene show the positive effect of amine basicity on the heptanoic acid production, which increases with pK_a augmentation of the amine ligand in absence of steric effect (present in the 2-picoline and 2,6-lutidine). The Rh/2,6-lutidine system displays the highest activity indicating that the electronic factor outweighs the steric. However, the WGSR data shows a different trend, the $Rh(4\text{-pic})_2$/P(4-PV) system being the most active.

In the absence of 1-hexene, this $Rh(amine)_2$/P(4-VP) system catalyzed the WGSR under the following reaction conditions: [Rh] = 2 wt.%, 10 mL of water, under P(CO) = 0.9 atm at 100 °C for 8 h. The $TF(H_2)$/day and $TF(CO_2)$/day observed values followed the order 4-picoline {15;15} > 3-picoline {12;12} > pyridine {10;11} ≥ 3,5-lutidine {10;10} > 2-picoline {8;9} > 2,6-lutidina {7;7} and is clearly evident that "$Rh(4\text{-pic})_2$" system displays the highest activity.

Interestingly in the presence of 1-hexene, decreases both $TF(H_2)$/day and $TF(CO_2)$/day can be observed. The most affected WGSR catalytic system is the "$Rh(2,6\text{-lut})_2$" and the less is the "$Rh(4\text{-pic})_2$". However, the $Rh(2,6\text{-lut})_2$ system is the most active for the catalytic hydroxycarbonylation of 1-hexene to heptanoic acid. These results can be interpreted as a competition process between the WGSR and the hydroxycarbonylation reactions.

The recycling efficiency of the immobilized "$Rh(4\text{-pic})_2$" catalyst was examined by reusing five more times the same catalyst previously used. The authors reported non significant changes of the hydroxycarbonylation catalytic activity after repetitive use (TF(acid) = 32, 27, 25, 26, and 27 day^{-1}, for the first, second, third, fourth and fifth use, respectively). These results show that this Rh immobilized catalyst has a high stability.

Pardey et al. [20b] proposed a mechanism for both the WGSR and 1-hexene hydroxycarbonylation (Scheme 11). The upper part of Scheme 10 shows the WGSR catalytic cycle (L = amine, P = P(4-VP)). Coordination of CO to the immobilized P-$[Rh(L)_2]^+$ (1) complex (step a) gives the electrophilic P-$[Rh(CO)(L)_2]^+$ species (2). The presence of P-$[Rh(CO)(L)_2]^+$ species was confirmed by FT-IR and XPS methods [10d,17]. Nucleophilic attack by H_2O on the coordinated CO, assisted by the free polymer (P) through its general base character, yields the hydroxycarbonyl P-$[Rh(CO_2H)(L)_2]$ species (3) and the protonated polymer PH^+ (step b). Elimination of CO_2 from the former species gives the hydride P-$[RhH(L)_2]$ (4) (step c), which

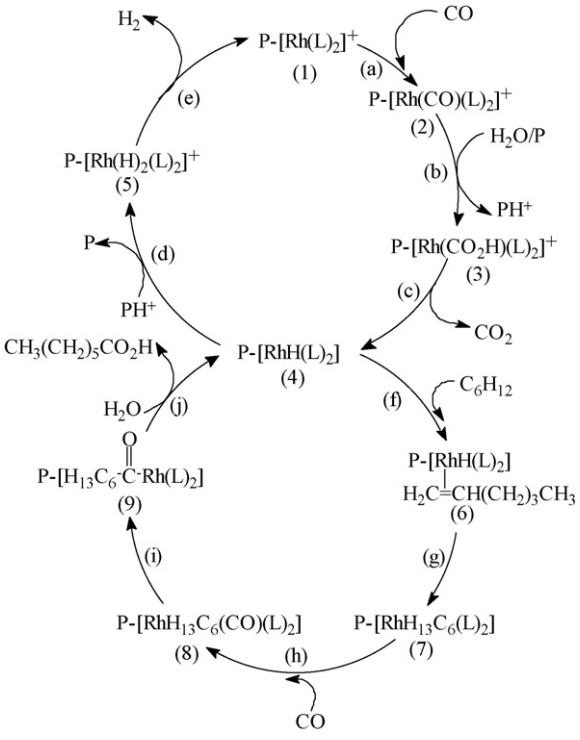

Scheme 11.

Table 7
Catalytic hydrocarbonylation of 1-hexene and WGSR by the $Rh(amine)_2$/P(4-VP) system in contact with CO/water.

Amine (pK_a)	$TF(H_2)$/day	$TF(CO_2)$/day	TF(acid)/day
Pyridine (5.27)	7	7	2
3-Picoline (5.52)	8	8	5
2-Picoline (5.97)	5	5	4
4-Picoline (6.00)	11	11	12
3,5-Lutidine (6.23)	6	6	15
2,6-Lutidine (6.75)	4	4	32

upon protonation by the pyridinium moiety PH^+ (step d) through its general acid character gives the dihydride complex P-[$Rh(H_2)(L)_2$] (5) and the free polymer (P). Reductive elimination of H_2 (step e) regenerates the starting P-[$Rh(L)_2$]$^+$ complex (1) and closes the WGSR cycle.

When 1-hexene is added to the previous WGSR catalytic active mixtures, the hydride P-[$RhH(L)_2$] complex (4) is intercepted by 1-hexene to give the olefin-rhodium P-[$RhH(L)_2$(1-hexene)] complex (6) (step f). Migratory insertion of the olefin into the Rh–H bond [20c] (step g) gives the alkyl-Rh complex (7), P-[$HRh(C_6H_{13})(L)_2$]. Further carbonylation by CO (step h) followed by migratory insertion of the alkyl ligand on the coordinated CO (step i) forms the acyl-Rh complex (9). The addition of a water molecule to (9) (step j) leads to the final elimination of the heptanoic acid and regeneration of the hydride P-[$RhH(L)_2$] complex (4) closing the hydroxycarbonylation cycle. Due to the strong acid conditions this step occurs *via* protonation of the acyl oxygen of complex (9) [20d], followed by the nucleophilic attack of a water molecule to the acyl carbon with the subsequent elimination of heptanoic acid, $CH_3(CH_2)_5CO_2H$, closing the hydroxycarbonylation cycle.

7. Hydroesterification and hydroformylation–acetalization of 1-hexene

7.1. Homogeneous systems

Pardey et al. [21] reported the catalysis of the hydroesterification and hydroformylation–acetalization of 1-hexene by rhodium(I) complexes, *cis*-[$Rh(CO)_2(amine)_2$](PF_6) (amine = pyridine, 2-picoline, 3-picoline, 4-picoline, 3,5-lutidine or 2,6-lutidine) dissolved in methanol under carbon monoxide atmosphere to give methyl-heptanoate and 1,1-dimethoxy-heptane as major products, and minor amounts of heptanal. The acetal product comes from the nucleophilic addition reaction of the methanol with the formed heptanal; also gaseous by-products H_2 and CO_2 coming from the catalysis of WGSR were observed. The results showed that TF(methyl-heptanoate)/day values depend on the nature of the coordinated amine and decrease in the order: 2,6-lutidine (21) > 3,5-lutidine (18) > 4-picoline (13) > 3-picoline (9) > pyridine (7) > 2-picoline (6) under the following catalytic conditions: [Rh] = (5×10^{-5} mol), [1-hexene] = 0.4 mL (3×10^{-3} mol), 1-hexene/Rh = 64, 10 mL (0.24 mol) of methanol, P(CO) = 0.9 atm at 100 °C for 4 h.

Accordingly, the catalytic hydroesterification of 1-hexene by these "Rh(amine)$_2$" complexes is influenced principally by the basic nature of the amine. Thus, the "Rh(2,6-lutidine)$_2$" system is the most active. The reverse order observed in the case of the "Rh(2-picoline)$_2$" system is due to the steric hindrance factor which overwhelms the electronic one. It is interesting to note that in "Rh(2,6-lutidine)$_2$" system the steric hindrance factor is not overwhelmed by the electronic factor even though the 2,6-lutidine amine is the most sterically hindered of all of the amines tested in this work.

However, the steric factor seems to control the observed tendency on the catalytic hydroformylation–acetalization of 1-hexene by these "Rh(amine)$_2$" systems. Based on the amounts ($\times 10^{-5}$ mol) of 1,1-dimethoxy-heptane formed it can be observed the following order 3-picoline (10.8) > 3,5-lutidine (8.4) > 4-picoline = pyridine (7.5) > 2-picoline = 2,6-lutidine (5.0). It seems that the hydroesterification of 1-hexene is more favored than hydroformylation–acetalization reactions by a factor ranging from 1.5- to 3.3-fold for the more basic amines, namely: 3,5-lutidine (60% yield of ester), 4-picoline (61% yield of ester) and 2,6-lutidine (77% yield of ester). However, the opposite tendency is observed when the amines are the less basic pyridine: (42% yield of ester) and 3-picoline (40% yield of ester); being the 2-picoline (49% yield of ester) in the borderline.

The authors also reported the effects of the reaction variables such as CO pressure, temperature, catalyst concentration, 1-hexene/Rh molar ratio and reaction medium on the catalysis, and the data were discussed in terms of catalytic cycles (Scheme 12). They concluded that common Rh–H catalytic species were involved.

Scheme 12 illustrates the proposed mechanism for the WGSR (A) and the hydroesterification (B) and the hydroformylation (C) reaction of 1-hexene by the highly and the stable "Rh(4-pic)$_2$" system. The amine ligands of the intermediate rhodium species were omitted for clarity. The proposed three-connected cycles *via* the {Rh(CO)(H)} intermediate species account for the observed products. Cycle (A) describes the formation of H_2 and CO_2 in a similar fashion as the WGSR cycle in Section 2, cycle (B) depicts the formation of methyl-heptanoate (ester) which comes from *in situ* methanolysis of the [Rh(CO)(acyl)] complex

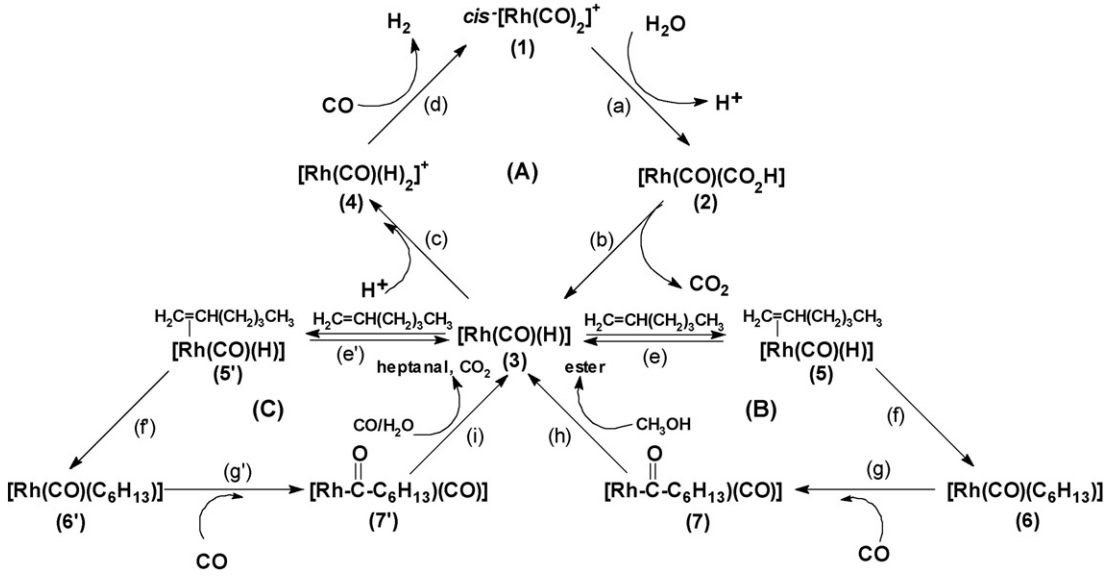

Scheme 12. Figure was reproduced from Ref. [22a], with permission of the copyright holders.

Table 8
Rhodium content effects on WGSR, hydroesterification and hydroformylation of 1-hexene in methanol, catalyzed by $Rh(4\text{-pic})_2$/P(4-VP) complex.

[Rh] wt.% ($\times 10^{-4}$ mol)	TF(CO_2)	TF(H_2)	TF(MH)	[Heptanal] ($\times 10^{-4}$ mol) (yield %)	[DMH] ($\times 10^{-4}$ mol) (yield %)
0.9 (0.5)	113	90	159	1.0 (2)	3.4 (4)
1.4 (0.8)	111	67	122	0.7 (1)	8.1 (11)
1.9 (1.1)	98	53	95	0.5 (1)	8.9 (14)
2.7 (1.5)	171	40	79	0.6 (1)	26.1 (29)
3.5 (1.9)	164	31	68	0.6 (1)	27.5 (33)
4.0 (2.2)	166	28	55	0.4 (1)	29.0 (35)
5.0 (2.8)	170	20	43	0.3 (1)	30.2 (38)

7 (step h). Cycle (C) illustrates the formation of heptanal which came from *in situ* hydrogenolysis of Rh-acyl complex 7(step i). Hydrogenolysis of the Rh-acyl intermediate, which leads to heptanal formation, probably comes from *intra*-hydrogen transfer from Rh–H species formed under conditions similar to the WGSR (cycle A).

7.2. Immobilized systems

Hung-Low et al. [22a] also reported the catalysis of the hydroesterification and hydroformylation–acetalization of 1-hexene by rhodium(I) $[Rh(cod)(amine)_2](PF_6)$ complexes (cod = 1,5-cyclooctadiene; amine = pyridine, 2-picoline, 3-picoline, 4-picoline, 3,5-lutidine or 2,6-lutidine) immobilized on P(4-VP) in contact with methanol under carbon monoxide atmosphere. In the presence of these immobilized complexes, 1-hexene, CO and methanol gave methyl-heptanoate and 1,1-dimethoxy-heptane as the main reaction products and minor amounts of heptanal. Additionally, gaseous by-products H_2 and CO_2 coming from the catalysis of WGSR were also observed.

Their results showed that TF(methyl-heptanoate) values depend on the nature of the coordinated amine and decrease in the order 4-picoline (58) > 3,5-lutidine (49) > 2,6-lutidine (39) > 2-picoline (25) > 3-picoline (21) > pyridine (13 $(24\,h)^{-1}$) at the following catalytic conditions: [Rh] = 1.9 wt.% (1×10^{-4} mol), 0.5 g of P(4-VP), [1-hexene] = 1.24 mL (1×10^{-2} mol), 1-hexene/Rh = 100, 10 mL (0.24 mol) of methanol, P(CO) = 0.9 atm at 100 °C for 5 h. The authors also reported the effects of the reaction variables such as CO pressure, temperature, 1-hexene/Rh molar ratio and reaction medium on the catalysis, and the data were discussed in terms of connected catalytic cycles through common Rh–H catalytic species and those cycles are similar to the previously described (Scheme 11) by the analogous homogeneous systems for the WGSR, hydroesterification and hydroformylation–acetalization reaction of 1-hexene [21] described above.

Hung-Low et al. [22b] reported the catalyst concentration effect on the WGSR, hydroesterification and hydroformylation–acetalization reaction of 1-hexene by the rhodium(I) $[Rh(cod)(4\text{-pic})_2](PF_6)$ complexes (cod = 1,5-cyclooctadiene) immobilized on P(4-VP) in contact with methanol under carbon monoxide atmosphere. Table 8 summarizes water-gas shift and hydrocarbonylation of 1-hexene rate data for the $Rh(4\text{-pic})_2$/P(4-VP) catalyst for the reaction conditions: [Rh] = 0.9–5.0 wt.%. The amount of 1-hexene was varied from 1.86 mL (1.5×10^{-2} mol) at [Rh] = 0.9 wt.% to 5.58 mL (4.5×10^{-2} mol) at [Rh] = 0.9 wt.% in order to keep the ratio [1-hexene]/[Rh] = 300 in all runs. [1-hexene] = 1.86–5.58 mL (1.5×10^{-2} to 4.5×10^{-2} mol), 1-hexene/Rh = 300, 10 mL (0.24 mol) of methanol, P(CO) = 20 atm at 110 °C for 5 h. TF(product) = [(mol of product)/(mol of Rh) × (rt)] × 24 h, where (rt) = reaction time in hours. MH = methyl-heptanoate. DMH = 1,1-dimethoxy-heptane.

Increasing [Rh] from 0.9 to 3.5 wt.% resulted in a decrease in both TF(MH) and TF(H_2), followed by nearly constant values at higher [Rh]. The results indicate that reaction rate is not first order

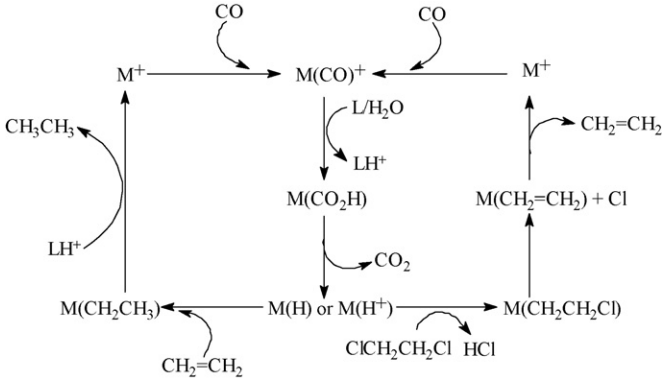

Scheme 13.

for both reactions in the [Rh] 0.9–5.0 wt.% range, and suggest that the active species may be present in several forms having different nuclearities. This suggestion is strongly supported by the FT-IR and XPS data reported for the immobilized $Rh(4\text{-pic})_2$/P(4-VP) WGSR catalysts, which show the presence of rhodium species with different nuclearities (mononuclear and polynuclear) and oxidation state (I) or (−I) [10d]. The oxidation state of the mononuclear and the polynuclear species are (I) and (−I), respectively. Further, mechanistic studies for WGSR catalyzed by this $Rh(4\text{-pic})_2$/P(4-VP) complex suggests a nucleophilic attack by water on the coordinated CO, assisted by free P(4-VP) yielding a hydroxycarbonyl Rh specie and a protonated polymer as a fundamental step [22c]. The negative charge of the anionic polynuclear complex increases the energy of this step and diminish the catalytic activity.

8. Hydrodechlorination of dichloroethane

Trabuco and Ford [23] examined homogeneous catalysts prepared from $RhCl_3$ in aqueous pyridine and substituted pyridines for the hydrodechlorination of 1,2-dicholoroethane to HCl, ethylene and ethane under the WGSR conditions. The conversion values (%) follows as 4-picoline = 3-picoline (34) > 2-picoline (7.5) > 2,6-lutidine (3.8) under (P(CO) = 0.9 atm at 100 °C for 22.5 h). The pattern of the hydrodechlorination of 1,2-dicholoroethane parallels the WGSR activities observed for the same solvent system [8]. They reported that the methyl groups in *meta*- and *para*-sites on pyridine increase the reactivity moderately, but methyl groups in the *ortho*-positions strongly inhibit the reactivity.

The same authors proposed two-connected catalytic cycles (Scheme 13), one related to reductive dechlorination of 1,2-dichloroethane to ethylene and HCl and the other related to hydrogenation of ethylene to ethane by CO/H_2O catalyzed by this rhodium-aqueous pyridine, bearing the same CO activation and M-H formation steps. In the proposed cycle the M–H or $M(H)^+$ species reduce the 1,2-dichloroethane to give an intermediate which undergo HCl elimination forming ethylene: In the other cycle

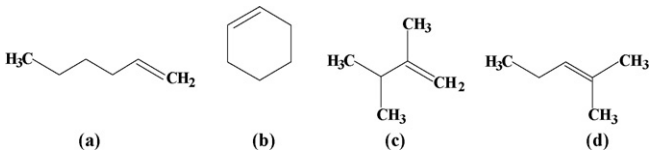

Fig. 14. Structure of: (a) 1-hexene, (b) cyclohexene, (c) 2,3-dimethyl-but-1-ene and (d) 2-methyl-pent-2-ene.

the insertion of ethylene to M–H bond occurs, affording intermediates which further form ethane.

9. Carbonylation of naphtha

The carbonylation of olefins present in naphtha constitute an alternative pathway to reduce the olefinic content in naphtha and to produce oxygenated products of greater added value which can be further used in a though be future industrial catalytic process for gasoline improving [24].

Pardey et al. [24c] reported the use of the immobilized [Rh(cod)(4-picoline)$_2$](PF$_6$)/P(4-VP) system in contact with methanol under carbon monoxide atmosphere as a catalyst for the carbonylation of some typical olefins present in a natural naphtha to oxygenated compounds.

The authors divided their studies in three steps: in the first step they carried out the individual carbonylation of 1-hexene, cyclohexene, 2,3-dimethyl-but-1-ene and 2-methyl-pent-2-ene (Fig. 14). These olefins were used as a model because they are generally present in major proportion among other olefins in real naphtha. The results for the carbonylation of this four olefin-model system show the following order (% of olefin conversion): 1-hexene (34) > 2,3-dimethyl-but-1-ene (28) > cyclohexene (26) > 2-methyl-pent-2-ene (3). Conditions: [Rh] = 2 wt.% (1.9×10^{-4} mol), 0.5 g of P(4-VP), 10 mL of CH_3OH, [olefin] = 1.9×10^{-2} mol, S/C = 100, P(CO) = 22 atm at 110 °C for 6 h.

The authors reported that under the described conditions, the catalytic carbonylation of 1-hexene gives methyl-heptanoate, heptanal, 2-methyl-hexanal, and 1,1-dimethoxy-heptane as the main reaction products. The catalytic carbonylation of cyclohexene gives methylcyclohexylmethanoate and cyclohexanecarbaldehyde. The catalytic carbonylation of 2-methyl-pent-2-ene and 2,3-dimethyl-but-1-ene give many oxygenated compounds such as esters (methyl-2,2-dimethylpentanoate and methyl-3,4-dimethyl-pentanoate), aldehydes (3,4-dimethyl-pentanal and 2,2-dimethylpentanal) and acetals (1,1-dimethoxy-3,4-dimethylpentane and 1,1-dimethoxy-2,2-dimethylpentane), among others. The methyl-heptanoate and methyl-cyclohexylmethanoate come from the 1-hexene and cyclohexene hydroesterification in methanol, respectively; the heptanal, 2-methyl-hexanal and cyclohexanecarbaldehyde come from the 1-hexene and cyclohexene hydroformylation and the 1,1-dimethoxy-heptane come from the nucleophilic addition between methanol and the formed heptanal, respectively. In addition formation of H_2 and CO_2 coming from the catalysis of the WGSR was observed.

Their data for the carbonylation of this four olefin-model system show that 2-methyl-pent-2-ene is the less reactive and for that reason, the authors focused the studies for achieving optimal conditions (reaction time (6–24 h), pressure of CO (22–33 atm) and temperature (80–130 °C)) for this olefin.

The rate-data indicate that optimal conditions for the catalytic carbonylation of 2-methyl-pent-2-ene by the Rh(4-pic)$_2$/P(4-VP) system are: [Rh] = 2 wt.% (1.9×10^{-4} mol), 0.5 g of P(4-VP), 10 mL of CH_3OH, [olefin] = 1.9×10^{-2} mol, S/C = 100, P(CO) = 33 atm at 110 °C for 24 h. These optimal values were used to examine the catalytic conversion for the rest of the individual olefins and the olefin conversion to carbonylated products (%) follows as: 1-hexene (63) > cyclohexene (50) > 2,3-dimethyl-but-1-ene (58) > 2-methyl-pent-2-ene (31). As it can be seen there is a substantial improvement in the conversion values for each individual olefin under these optimal reaction conditions.

In the second step they made a quaternary mixture (1-hexene, 45 wt.%; cyclohexene, 20 wt.%; 2,3-dimethyl-but-1-ene, 20 wt.%; and 2-methyl-pent-2-ene, 15 wt.%) and performed the catalytic carbonylation under the optical conditions previously determined in the first step. Table 9 shows the results under the optimal conditions reported above. Interestingly, this quaternary mixture shows a similar pattern of product formation as the observed with the individual olefins. In addition, formation of H_2 (TF(H_2) = 30 day^{-1}) coming from the WGSR was also observed.

In the third step the catalytic carbonylation of real Venezuelan naphtha was studied under the optimal reaction conditions ([Rh] = 2 wt.% (1.9×10^{-4} mol), 0.5 g of P(4-VP), 10 mL of methanol, [olefin] = 1.9×10^{-2} mol, S/C = 100, P(CO) = 33 atm at 110 °C for 24 h). GC analysis from the naphtha after of the catalytic reaction reveals the diminution of the olefin content and the increases of the amount of oxygenated products in the cut. Remarkably this approximation constitutes a potential promissory work for a future industrial catalytic process for gasoline improving based on *in situ* olefin carbonylation type reaction.

10. Hydrogenation and hydroformylation of alkenes

Ford and co-workers [25a] examined the hydrogenation and hydroformylation of 1-hexene and cyclohexene catalyzed by $RhCl_3$ immobilized on poly(4-vinylpyridine) in contact with aqueous 2-ethoxyethanol under mild WGSR conditions.

The authors reported the conversion of cyclohexene to cyclohexane and cyclohexane carboxaldehyde and 1-hexene to hexane, heptanal, 2-methylhexanal and *cis*- and *trans*-2-hexene under numerous experimental variables conditions (reaction time = 5–40 h, [cyclohexene] = 0.5–2.0 M, [1-hexene] = 0.25–1.5 M, P(CO) = 0–1.5 atm, T = 85–120 °C). The last two products come from the catalytic isomerization reaction of the 1-hexene. In addition, formation of H_2 coming from the catalysis of the WGSR by this Rh/P(4VP) system was observed.

The same authors reported a detailed kinetics investigation for both alkenes. The effect of cyclohexene concentration on hydrogenation, hydroformylation and WGSR was investigated and results showed equal amounts formation of cyclohexane and cyclohexane carboxaldehyde in the range studied. This behavior is consistent with formation of an intermediate which can be partitioned to give the two organic products. However,

Table 9
Carbonylation of quaternary olefin mixture by [Rh(4-pic)$_2$]/P(4-VP) catalyst.

Total conversion of the mixture (%)	Individual components (wt.%)	Products
51	1-Hexene (45) 2,3-Dimethyl-1-butene (20) Cyclohexene (20) 2-Methyl-2-pentene (15)	Methyl-heptanoate, heptanal, 2-methyl-hexanal and 1,1-dimethoxy-heptane 3,4-Dimethyl-pentanal, methyl-3,4-dimethyl-pentanoate and 1,1- dimethoxy-3,4-dimethyl-pentane Cyclohexylmethanal, methyl-cyclohexylmetanoate and dimethoxy-cyclohexylmetane 2,2-Dimethylpentanal, methyl-2,2-dimethylpentanoate, and 1,1-dimethoxy-2,2-dimethylpentane

formation of H_2 decreases as the cyclohexene concentration increases. These results indicated a competition between organic products formation and H_2 production which is [cyclohexene] dependent.

The rate data display curvatures for H_2 and cyclohexane formation and aldehyde production leveled off at high P(CO) (P(CO) < 1 atm). The authors suggested that the CO activation occurred through a pre-equilibrium formation of P–Rh–CO species followed by slower reaction to give WGSR products. However, since TF(cyclohexane) and TF(H_2) values decreases at higher P(CO) and TF(aldehyde) level out a more complex mechanism is needed to explain the observer role of P(CO).

Temperature effects on the catalytic hydrogenation and hydroformylation of cyclohexene displays segmented Arrhenius plot and exhibit inflection points at 100 °C. The apparent activation energies obtained from the slopes for hexane formation are 10.2 kcal/mol at temperatures < 100 °C and 31 kcal/mol at temperatures > 100 °C. The apparent activation energies obtained from the slopes for aldehyde formation are 5.4 kcal/mol at temperatures < 100 °C and 22 kcal/mol at temperatures > 100 °C. Arrhenius plots that are segmented indicate a change in the rate limiting step between two competitive reactions [25b].

The effect of 1-hexene concentration on hydrogenation, hydroformylation and isomerization was investigated and results showed that the isomerization of 1-hexene to *cis*- and *trans*-2-hexene was most rapid transformation as those results are consistent with the literature data for Rh catalyst [25c]. This behavior is consistent with formation of an intermediate which can be partitioned to give the two organic products. However, formation of H_2 decreases as the cyclohexene concentration increases. These results indicated a competition between organic products formation and H_2 production which is [cyclohexene] dependent.

The rate data display curvatures for H_2 and cyclohexane formation and aldehyde production leveled off at high P(CO) (P(CO) < 1 atm). The authors suggested that the CO activation occurred through a pre-equilibrium formation of P–Rh–CO species followed by slower reaction to give WGSR products. However, since TF(cyclohexane) and TF(H_2) values decreases at higher P(CO) and TF(aldehyde) level out a more complex mechanism is needed to explain the observer role of P(CO).

Temperature effects on the catalytic hydrogenation and hydroformylation of cyclohexene displays segmented Arrhenius plots and exhibit inflection points at 100 °C. The apparent activation energies obtained from the slopes for cyclohexane formation are 10.2 kcal/mol at temperatures < 100 °C and 31 kcal/mol at T > 100 °C. The apparent activation energies obtained from the slopes for cyclohexane carboxaldehyde formation are 5.4 kcal/mol at temperatures < 100 °C and 22 kcal/mol at T > 100 °C.

The 1-hexene hydrogenation, hydroformylation, isomerization and WGSR were also investigated and shows that isomerization of this olefin is the most rapid transformation. The *cis*- and *trans*-2-hexene were the principal isomers (*cis*/*trans* = 0.45) produced. The effect of [1-hexene] on the TF values reveals that at low substrate concentrations the TF values increased, but TF(aldehyde) values leveled out for [1-hexene] = >0.25 M. The TF values for isomerization and hydrogenation increased with [1-hexene] in a nonlinear fashion.

The effect of P(CO) on the TF values reveals that at higher P(CO) the TF for isomerization and hydroformylation values increased in the entire range (0.5–1.5 atm). The TF(H_2) values increase up to 0.5 atm, then undergo a decrease at higher P(CO). Furthermore, the value of the ratio linear/branched aldehyde changed with P(CO) from 0.6 (0.3 atm) to 1.5 (1.5 atm). This behavior could be related to the better tramping of CO through migratory insertion path for a terminally bound alkyl which leads to the formation of the linear isomer.

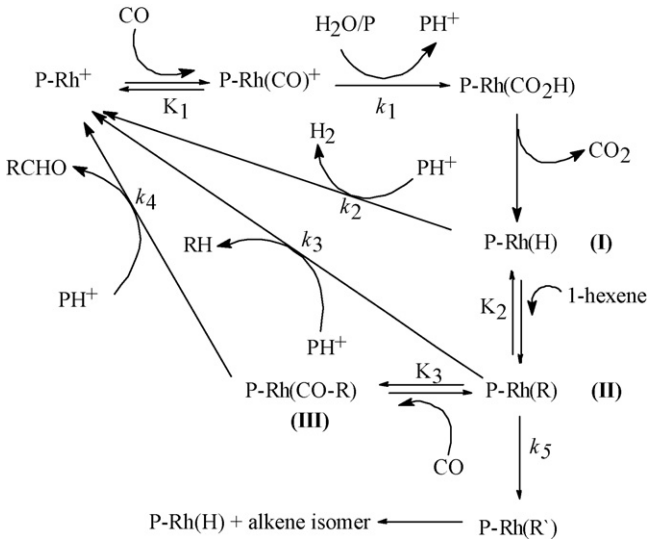

Scheme 14. P = free P(4-VP).

The catalytic hydrogenation, isomerization and hydroformylation of 1-hexene also display segmented Arrhenius plots and exhibit inflection points at 100 °C. The apparent activation energies obtained from the slopes for hexane formation are 15.1 kcal/mol at T < 100 °C and 30.8 kcal/mol at T > 100 °C. The apparent activation energies obtained from the slopes for heptanal and 2-methylhexanal formation are 4.5 kcal/mol at T < 100 °C and 13.9 kcal/mol at T > 100 °C. The apparent activation energies obtained from the slopes for 2-hexene formation are 2.0 kcal/mol at T < 100 °C and 16.3 kcal/mol at T > 100 °C.

The results shows that this Rh/P(4-VP) system favors hydrogenation over hydroformylation under the mild WGSR conditions used in this study. Similar behavior was previously noted for other rhodium system [25c].

The authors proposed the following reaction scheme (Scheme 14) to describe the catalysis for these two alkenes substrates.

Based on the kinetics studies it can be assumed some kind of faster interchange between the three intermediates I, II and III in Scheme 14 than the pathway leading to the WGSR, alkene hydrogenation and alkene hydroformylation allowing these species to be in equilibrium. If CO activation *via* the k_1 step were the rate limiting the individual rates of the three catalytic processes should be determined by the relative concentrations of these three species as well the individual rate constant. It was shown that the TF for the three processes were P(CO) dependent. Accordingly, this scheme describes qualitative these observations. In addition, the authors describe a complex quantitative model, which fix with the hypothetical Scheme 14.

Pardey and co-workers [25d] reported catalytic studies of the hydroformylation and the isomerization of 1-hexene to aldehydes (heptanal and 2-methyl-hexanal) and 2-hexene, respectively by [Rh(COD)(amine)$_2$]PF_6 complexes (COD = 1,5-cyclooctadiene, amine = 4-picoline, 2-picoline or 2,6-lutidine) immobilized on poly(4-vinylpyridine) in contact with 10 mL of 80% aqueous 2-ethoxyethanol, under CO atmosphere (0.9 atm at 100 °C). The results of these studies show the Turnover Frequencies for aldehydes production follows the order: 2-picoline (2.9) > 4-picoline (2.6) > 2,6-lutidine (2.4). The electronics and steric effects induced by the amine ligands apparently influence on the observed catalytic activities.

The same group [25e] examined the influence of the reaction conditions variation (1-hexene/Rh molar ratio = 16–105, tempera-

Table 10
Effect of 1-hexene/Rh molar ratio (S/C), CO pressure (P(CO)), and temperature (*T*) on WGSR and 1-hexene isomerization and hydroformylation catalysis by [Rh(cod)(2-pic)2](PF_6) immobilized on P(4-VP).

1-Hexene (mL)	S/C	P(CO) (atm)	*T* (°C)	TF(CO_2)	TF(H_2)	TF(Iso)	TF (Ald)
0.2	16	0.9	100	11.0	3.6	6.3	1.1
0.4	32	0.9	100	14.2	2.3	10.1	1.8
0.6	49	0.9	100	17.4	2.1	13.0	2.3
0.8	65	0.9	100	18.5	2.1	13.9	2.5
1.3	105	0.9	100	20.1	1.2	16.1	2.8
1.3	105	0.6	100	14.3	0.4	12.3	1.5
1.3	105	1.2	100	22.7	2.5	17.2	3.1
1.3	105	1.5	100	24.4	2.4	18.9	3.3
1.3	105	1.8	100	21.9	3.5	15.7	3.4
1.3	105	0.9	70	5.8	0.2	4.8	0.9
1.3	105	0.9	80	10.6	0.7	8.5	1.5
1.3	105	0.9	90	19.2	1.0	15.5	2.7
1.3	105	0.9	110	29.3	2.6	22.6	4.0

ture = 70–110 °C and carbon monoxide pressure = 0.6–1.8 atm) on the catalytic hydroformylation and isomerization of 1-hexene catalyzed by [Rh(cod)(2-picoline)$_2$](PF_6) (cod = 1,5-cyclooctadiene) immobilized on poly(4-vinylpyridine) in contact with 80% aqueous 2-ethoxyethanol under mild WGSR conditions (Eq. (11)). Formation of methyl-heptanoate, heptanal, 2-hexene, H_2 and CO_2 were observed. The results are shown in Table 10 for the reaction conditions: 0.5 g of P(4-VP), [Rh] = 2.0 wt.%, 8 mL of 2-ethoxyethanol, 2 mL of H_2O. TF(product) = mol of product $(\text{mol Rh} \times 24\,\text{h})^{-1}$. Ald = aldehydes, Iso = isomerization:

$$\text{R–CH=CH}_2 + 2\text{CO} + \text{H}_2\text{O} \rightarrow \text{R–CH}_2\text{CH}_2(\text{HCO}) + \text{CO}_2 \quad (11)$$

The TF(Ald) increased from 1.1 (S/C = 16) to 2.8 $(24\,\text{h})^{-1}$ (S/C = 105) and the TF(H_2) values decreased from 3.6 (S/C = 16) to 1.2 $(24\,\text{h})^{-1}$ (S/C = 105). These results indicate that the concentration of the Rh species responsible for the catalysis of the WGSR decreased in presence of 1-hexene due to an apparent competition between hydroformylation and the WGSR or by to the shift of the equilibrium back (Eq. (1)) by the CO_2 also formed in the hydroformylation reaction. Interestingly, hydrogenation of 1-hexene and/or 2-hexene to hexane and hydrogenation of heptanal and 2-methyl-hexanal to the corresponding alcohols was not observed even though formation of H_2.

The catalytic hydroformylation of 1-hexene also display segmented Arrhenius plots and exhibit inflection points at 90 °C. The apparent activation energies obtained from the slopes for aldehydes formation are $123.3 \pm 12.3\,\text{kJ mol}^{-1}$ at $T < 90$ °C and $53.7 \pm 5.4\,\text{kJ mol}^{-1}$ at $T > 100$ °C. Arrhenius plots, which are concave upwards, suggest a change in the rate-limiting step between two competitive reactions [25b].

Both the hydroformylation and isomerization rate of 1-hexene increase with P(CO) to *ca.* 1.2 atm. Above 1.2 atm of CO, the isomerization of 1-hexene is inhibited and the formation of aldehydes appears to be independent of CO pressure in the 1.2–1.8 atm ranges. However, the formation of H_2 increases almost linearly in the whole ranges. The hydroformylation behavior is consistent with a mechanism in which the rate-limiting step is preceded by reversible coordination of CO to Rh immobilized species followed by a slower reaction to give the products (Eq. (12)), *e.g.*

$$\text{P-[Rh]}^{+} \overset{K}{\rightleftarrows} \text{P-[Rh–CO]}^{+} \overset{k_1\ \text{1-hexene/H}_2\text{O}}{\longrightarrow} \text{P-[Rh]}^{+} + \text{CO}_2 + \text{products} \quad (12)$$

Interesting, the presence of the 2-picoline ligands in the Rh(2-pic)$_2$/P(4-VP) system precludes the catalytic hydrogenation step observed in the $RhCl_3$/P(4-VP) catalytic system. The Scheme 15 describes the catalysis for the observed reactions.

Scheme 15 derives from Scheme 14. The hydrogenation step from Scheme 14 is obviated in Scheme 14 because hydrogenation of 1-hexene was not observed for the Rh(2-Pic)$_2$/P(4-VP) catalytic system.

Based on TF dependence on P(CO) and the step k_1 as the rate limiting it is assumed a faster interchange between the three intermediates (I), (II) and (III) in Scheme 14. Accordingly, the individual rates for the WGSR and hydroformylation of 1-hexene should be determined by the relative concentrations of these three species as well the individual rate constant.

11. Catalysis by iridium complexes bearing pyridine ligands

In this section some examples of soluble and immobilized complexes of iridium bearing pyridine ligands have shown as catalysts will be described.

Pardey and coworkers reported WGSR activity for the iridium complexes, *cis*-[Ir(CO)$_2$(amine)$_2$](PF_6) [26a]. TF(H_2) values follows the order 4-picoline (14) > 3-picoline (10) > pyridine (9) > 3,5-lutidine (9) > 2-picoline (4) > 2,6-lutidine (3) under 1.9 atm of CO at 100 °C; [Rh] = 10 mM, 10 mL of 80% aqueous amine. The authors suggest an electronic and steric influence. Kinetics studies carried out for the same group [26b] reveals that the catalysis proved to be non-linear dependence in [Ir] over the 5–80 mM range. The authors suggested the presence of active mononuclear and polynuclear Ir species. In addition the rate displays a first order dependence on P(CO), over the 0.7–1.9 atm range. The authors proposed a CO addition to the catalyst species prior to rate-limiting step. A mechanistic cycle was proposed (Scheme 16).

In addition, *in situ* FT-IR and ^{13}C NMR spectroscopic studies of the complex *cis*-[Ir(CO)$_2$(py)$_2$](PF_6) (py = pyridine) dissolved in 80%

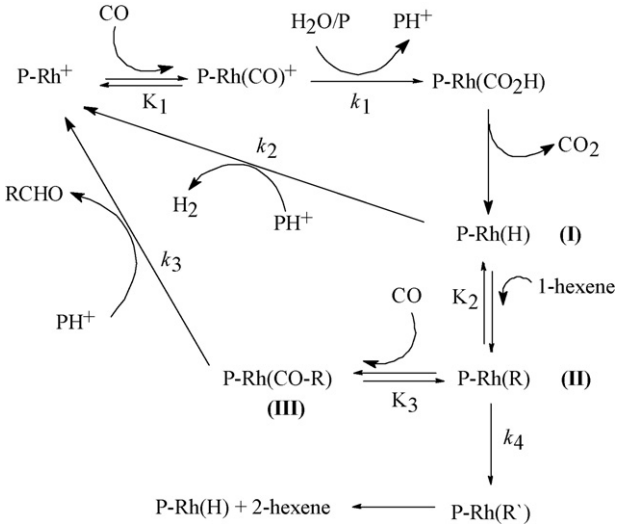

Scheme 15. P = free P(4-VP).

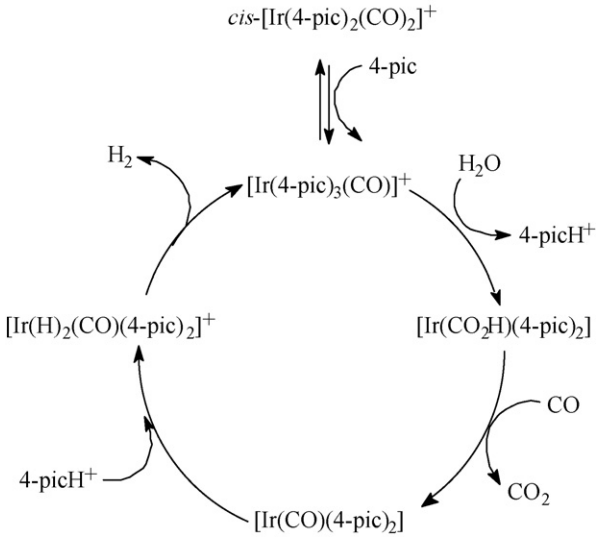

Scheme 16.

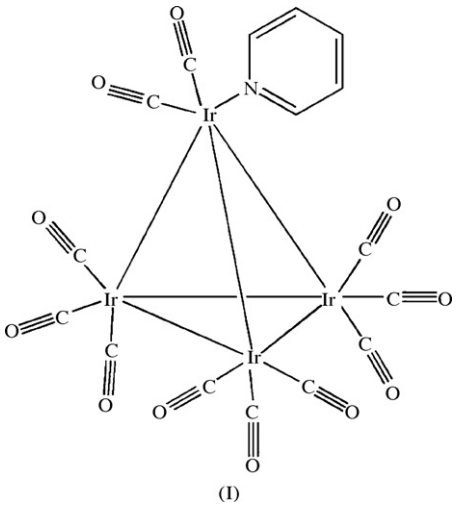

Fig. 15. Molecular structure of $Ir_4(CO)_{11}(py)$ complex.

aqueous pyridine used as a precursor in WGSR were carried out [26c]. These spectroscopy studies reveal the presence of aminocarbonyliridium complexes with linear and bridging carbonyls groups as reaction intermediates. The $Ir_4(CO)_{12}$ complex was also examimate in 4-picoline and displayed a $TF(H_2) = 12\ (24\,h)^{-1}$ [26c]. Interestingly, from the catalytic conditions was isolated a solid which its crystal structure (Fig. 15) was determined [26d].

This cluster maintains its tetrahedral Ir_4 core and each octahedral Ir centre is attached to three other Ir atoms and three carbonyl groups, except for one Ir atom, which is bound to only two carbonyl ligands with the third site occupied by the pyridine N atom.

The *cis*-$[Ir(CO)_2(amine)_2](PF_6)$ system also show catalytic activities for nitrobenzene reduction to aniline under CO/H_2O [26e]. Aniline production (mmol) values follow the order 4-picoline (0.119) > 2-picoline (0.066) > 2,6-lutidine (0.046) > 3-picoline (0.044) > pyridine (0.043) > 3,5-lutidine (0.040) under 1.9 atm of CO at 100 °C; [Rh] = 10 mM, 10 mL of 80% aqueous amine.

12. Summary

In this short review, a survey of soluble and immobilized complexes of rhodium with pyridine ligands have shown the versatility and utility of these compounds as catalysts in reactions as varied as the WGSR, the carbonylation of methanol to acetic acid and its ester, the reduction of nitroarenes to the corresponding anilines, the oligomerization and hydrocarboxylation of CO/ethylene to ketones and propionic acid, hydrocarbonylation of 1-hexene to heptanoic acid, the hydroesterification and hydroformylation-acetalization of 1-hexene to carbonylated products, the hydrodechlorination of 1,2-dicholoroethane to ethylene, the carbonylation of naphtha to oxygenated products and the hydrogenation and hydroformylation of alkenes to alkanes and aldehydes. The catalytic activity of these metal complexes is significant and the systematic studies carried out with this kind of complexes have been possible to propose catalytic mechanisms.

It was shown in the above described examples, in general, the positive effect of N-donor ligand basicity on catalytic activity which increases with pKa augmentation of the N-donor ligand in absence of steric effect; namely, the coordination of the substrate to the Rh center is a crucial step, and it can be inhibited in some degree by the effective block of methyl groups in *ortho*-position to N-atom of the aromatic ring and consequently decreasing the catalytic activity. Also, the blocking effect can prevent or decrease the rate of other elementary reactions of the catalytic cycle, which require an open coordination site on the metal center. However, in the case of the reduction of nitroarenes by the Rh/hindered amine ligands catalytic system this kind of block serves to creates reservoirs of Rh–H species, which consequently leads to the observed high activity. In those cases the steric effect overcomes the electronic one.

Acknowledgment

The authors thank the Fonacit-Venezuela (S1-2002000260) and CDCH-UCV (PG-03-00-6928-2007) for the financial support. Special thanks to Prof. Peter C. Ford for valuable discussions.

Appendix A. List of abbreviations

aq.	aqueous
BET	methods for determining surface area (Brunauer, Emmett and Teller).
cod	1,5-cyclooctadiene
dppe	1,2-bis(diphenylphosphino)ethane
DTA–TGA	differential thermal analysis and thermo gravimetric analysis
EPR	electron paramagnetic spectroscopy
FT-IR	Fourier transform infrared spectroscopy
NMR	nuclear magnetic resonance
4-pic	4-picoline or 4-methylpyridine
2-pic	2-picoline or 2-methylpyridine
P(4-VP)	poly(4-vinylpyridine)
py	pyridine
RNO_2	nitrobenzene
SEM–EDX	scanning electron microscopy with energy dispersive X-ray
S/C	substrate/catalyst
TMEDA	N,N,N′,N′-tetramethylethylenediamine
TF	turnover frequency
TON	turnover number
UV–Vis	ultraviolet–visible
WGSR	water-gas shift reaction
XPS	X-ray photoelectron spectroscopy

References

[1] (a) A. Togni, L.M. Venanzi, Angew. Chem. Int. Ed. Engl. 33 (1994) 497;
(b) J.D. Petersen, W.R. Murphy, R. Sahai, K.J. Brewer, R.R. Rumenski, Coord. Chem. Rev. 261 (1985) 64;

(c) R.G. Pearson, J. Am. Chem. Soc. 85 (1963) 3533;
(d) R.G. Pearson, Science 151 (1966) 172;
(e) R.G. Pearson, Chem. Brit. 3 (1967) 103;
(f) R.G. Pearson, J. Chem. Ed. 64 (1987) 561;
(g) R.G. Pearson, Chemical Hardness: Applications from Molecules to Solids, Wiley–VCH, Weinheim, 1999;
(h) P.A. Lay, Inorg. Chem. 23 (1984) 4775.
[2] (a) P. Fougeroux, B. Denise, R. Bonnaire, G. Pannetier, J. Organomet. Chem. 60 (1973) 375;
(b) B. Denise, G. Pannetier, J. Organometal. Chem. 63 (1973) 423.
[3] L.M. Vallarino, S.W. Seargold, Inorg. Chim. Acta 36 (1979) 243.
[4] T. Najat, F. Barbirm, Hydrogen Energy Technologies, UNIDO Emergent Technologies Series, Viena, 1998.
[5] (a) P.C. Ford, Acc. Chem. Res. 14 (1981) 31;
(b) M. Laine, R.B. Wilson Jr., in: R. Ugo (Ed.), Aspects of Homogeneous Catalysis, vol. 5, Reidel, Dordrecht, 1984, p. 217;
(c) P.C. Ford, A. Rokicki, Adv. Organomet. Chem. 28 (1988) 139;
(d) R.M. Laine, E.J. Crawford, J. Mol. Catal. 44 (1988) 357;
(e) G. Jacobs, B.H. Davis, in: J.J. Catalysis, K.M. Spivey, Dooley (Eds.), Low Temperature Water-gas Shift Catalysts, vol. 20, RSC Publishing, Cambridge, UK, 2007, p. 122.
[6] (a) C. Ungermann, V. Landis, S.A. Moya, H. Cohen, H. Walker, R.G. Pearson, R.G. Rinker, P.C. Ford, J. Am. Chem. Soc. 101 (1979) 5922;
(b) R.G. Pearson, H. Mauermann, J. Am. Chem. Soc. 104 (1982) 500.
[7] K. Kaneda, M. Hiraki, K. Sano, T. Imanaka, S. Teranishi, J. Mol. Catal. 9 (1980) 227.
[8] A.J. Pardey, P.C. Ford, J. Mol. Catal. 53 (1989) 247.
[9] (a) G. Fachinetti, G. Fochi, T. Funaioli, Inorg. Chem. 33 (1994) 1719;
(b) G. Fachinetti, T. Funaioli, J. Organomet. Chem. 460 (1994) C34;
(c) J.P. Collin, R. Ruppert, J.P. Sauvage, Nouveau J. Chim. 9 (1985) 395.
[10] (a) M. Mdleleni, R. Rinker, P.C. Ford, J. Mol. Catal. 89 (1994) 283;
(b) A.J. Pardey, M. Mediavilla, M. Canestrari, D. Moronta, C. Urbina, E. Lujano, P. Baricelli, C. Longo, R. Pastene, S.a. Moya, Catal. Lett. 56 (1998) 231;
(c) A.J. Pardey, M. Fernández, M. Canestrari, P. Baricelli, E. Lujano, C. Longo, R. Sartori, S.a. Moya, React. Kinet. Catal. Lett. 67 (1999) 325;
(d) A.J. Pardey, M. Fernández, J. Alvarez, C. Urbina, D. Moronta, V. Leon, M. Haukka, T.A. Pakkanen, Appl. Catal. A 199 (2000) 275;
(e) M. Mdleleni, R. Rinker, P.C. Ford, Inorg. Chim. Acta 270 (1998) 345.
[11] (a) N. Kumari, M. Sharma, P. Das, D.K. Dutta, Appl. Organomet. Chem. 16 (2002) 258;
(b) M.J. Howard, M.D. Jones, M.S. Roberts, S.A. Taylor, Catal. Today 18 (1993) 325;
(c) N. Kumari, M. Sharma, P. Chutia, D.K. Dutta, J. Mol. Catal. A 222 (2004) 53;
(d) J.C. Jeffrey, T.B. Rauchfuss, Inorg. Chem. 18 (1979) 2658;
(e) D.K. Dutta, J.D. Woollins, A.M.Z. Slawin, D. Konwar, P. Das, M. Sharma, P. Bhattacharyya, S.M. Aucott, J. Chem. Soc. Dalton Trans. (2003) 2674;
(f) N. Kumari, B.J. Sarmah, D.K. Dutta, J. Mol. Catal. A 266 (2007) 260;
(g) H. Kiyono, K. Inoue, H. Takeuchi, S. Konaka, J. Mol. Struct. 476 (1999) 73;
(h) J. Rankin, A.D. Poole, A.C. Benyei, D.J. Cole-Hamilton, J. Chem. Soc. Chem. Commun. (1997) 1835;
(i) B.J. Sarmah, J. Bibek, B. Borah, D.K. Deb, Dutta, J. Mol. Catal. A 289 (2008) 95;
(j) D.K. Dutta, P. Chutia, B.J. Sarmah, B.J. Borah, B. Deb, J.D. Woollins, J. Mol. Catal. A 300 (2009) 29;
(k) M. Sharma, B.J. Sarmah, P. Bhattacharyya, R.C. Dekaand, D.K. Dutta, Appl. Organomet. Chem. 21 (2007) 255.
[12] (a) D. Foster, Adv. Organomet. Chem. 17 (1979) 255;
(b) P.M. Maitlis, A. Haynes, G.J. Sunley, M.J. Howard, J. Chem. Soc. Dalton Trans. (1996) 2187.
[13] (a) C. Linares, M. Mediavilla, A.J. Pardey, P. Baricelli, C. Longo-Pardey, S.a. Moya, Catal. Lett. 50 (1998) 183;
(b) C. Longo, J. Alvarez, M. Fernández, A.J. Pardey, S.a. Moya, P. Baricelli, M.M. Mdleleni, Polyhedron 19 (2000) 487.
[14] (a) F. Ragaini, S. Cenini, F. Demartin, J. Chem. Soc. Chem. Commun. (1992) 1467;
(b) S.J. Skoog, J.P. Campbell, W.L. Gladfelter, Organometallics 13 (1994) 4137;
(c) S.J. Skoog, W.L. Gladfelter, J. Am. Chem. Soc. 119 (1997) 11049.
[15] M.M. Mdleleni, R.G. Rinker, P.C. Ford, J. Mol. Catal. A 204–205 (2003) 125.
[16] (a) C. Fernández, E. Lujano, U. Macias, J. Marcano, P.J. Baricelli, C. Longo, S.A. Moya, M.G. Solórzano, M.C. Ortega, A.J. Pardey, Catal. Lett. 95 (2004) 143;
(b) US Department of Health and Human Services, National Toxicology Program, Technical Report Series No. 442, 1994.
[17] (a) A.J. Pardey, M. Fernández, J. Alvarez, C. Urbina, D. Moronta, V. Leon, C. Longo, P. Baricelli, S.A. Moya, J. Mol. Catal. A 164 (2000) 225;
(b) M.P. McCurdie, L.A. Belfiore, Polymer 40 (1999) 2889;
(c) K. Nakamoto, Infrared and Raman Spectra of Organic and Coordination Compounds, Wiley, New York, 1997;
(d) C. Giacomelli, F.C. Giacomelli, A.L. Santana, V. Schmidt, A.T. Nunes-Pires, J.R. Bertolino, A. Spinelli, J. Braz. Chem. Soc. 15 (2004) 818;
(e) A.M. Dennis, R.A. Howard, K.M. Kadish, J.L. Bear, Inorg. Chim. Acta 44 (1980) L139;
(f) A.J. Pardey, M. Fernández, A.B. Rivas, M.C. Ortega, C. Urbina, D. Moronta, C. Longo, M. Mediavilla, P.J. Baricelli, S.A. Moya, Inorg. Chim. Acta 329 (2002) 22;
(g) P. Uguagliati, G. Deganello, U. Belluco, Inorg. Chim. Acta 9 (1974) 203;
(h) A.J. Pribula, R.S. Drago, J. Am. Chem. Soc. 98 (1976) 2784.
[18] A.J. Pardey, C. Longo, T. Funaioli, G. Fachinetti, Polyhedron 23 (2004) 1683.
[19] (a) Y. Iwashita, M. Sakuraba, Tetrahedron Lett. 26 (1971) 2409;
(b) P.A. Lay, Inorg. Chem. 23 (1984) 4775.
[20] (a) F. Hung-Low, G.C. Uzcátegui, J. Alvarez, M.C. Ortega, A.J. Pardey, C. Longo, React. Kinet. Catal. Lett. 84 (2005) 87;
(b) A.J. Pardey, F. Hung-Low, G.C. Uzcátegui, M.C. Ortega, C. Longo, React. Kinet. Catal. Lett. 88 (2006) 203;
(c) G. Consiglio, Chimia 55 (2001) 809;
(d) F. De Angelis, S. Sgamellotti, Organometallics 19 (2000) 4104.
[21] A.J. Pardey, G.C. Uzcátegui, F. Hung-Low, A.B. Rivas, J.E. Yánez, M.C. Ortega, J. Alvarez, C. Longo, P. Aguirre, S.A. Moya, J. Mol. Catal. A 239 (2005) 205.
[22] (a) F. Hung-Low, G.C. Uzcátegui, M.C. Ortega, A.B. Rivas, J.E. Yánez, J. Alvarez, A.J. Pardey, C. Longo, Catal. Today 107–108 (2005) 273;
(b) F. Hung-Low, G.C. Uzcátegui, J. Alvarez, M.C. Ortega, A.J. Pardey, C. Longo, React. Kinet. Catal. Lett. 88 (2006) 143;
(c) A.J. Pardey, M. Fernández, J. Alvarez, M.C. Ortega, M. Canestrari, C. Longo, P. Aguirre, S.A. Moya, E. Lujano, P.J. Baricelli, Bol. Soc. Chil. Quím. 45 (2000) 347.
[23] E. Trabuco, P.C. Ford, J. Mol. Catal. A 148 (1999) 1.
[24] (a) M. Reyes, D. Mercades, B. Fontal, T. Suárez, F. Bellandi, R.R. Contreras, I. Romero, Y. Fonseca, P. Cancines, React. Kinet. Catal. Lett. 90 (2007) 347;
(b) M. Reyes, E.J. Parra, Y. Fonseca, B. Fontal, T. Suárez, F. Bellandi, R.R. Contreras, I. Romero, L. Prado, P. Cancines, Av. Quim. 3 (2008) 15;
(c) A.J. Pardey, J.D. Suárez, G. Gascón, M.C. Ortega, C. Longo, S.A. Moya, Catal. Lett. 126 (2008) 112;
(d) V.J. Guanipa, Q.L.G. Melean, M. Madroño-Alonzo, A. Gonzalez, M. Rosales, F. Lopez-Linares, P.J. Baricelli, Appl. Catal. A 358 (2009) 21;
(e) M. Madroño-Alonzo, V.J. Guanipa, L.G. Melean, M. Rosales, A. Gonzalez, P.J. Baricelli, Appl. Catal. A 358 (2009) 211.
[25] (a) M.M. Mdleleni, R.G. Rinker, P.C. Ford, Inorg. Chim. Acta 270 (1998) 345;
(b) A.A. Frost, R.G. Pearson, Kinetics and Mechanism, Wiley, New York, 1961, p. 24;
(c) T. Okana, T. Kobayashi, H. Konishi, Bull. Chem. Soc. Jpn. 54 (1981) 3799;
(d) A.J. Pardey, J. Brito, A.B. Rivas, M.C. Ortega, C. Longo, P.J. Baricelli, E. Lujano, M. Yañez, C. Zuñiga, R. López, S.A. Moya, J. Chil. Chem. Soc. 48 (2003) 57;
(e) A.J. Pardey, J. Brito, M. Fernández, A.B. Rivas, M.C. Ortega, C. Longo, P.J. Baricelli, E. Lujano, S.A. Moya, React. Kinet. Catal. Lett. 74 (2001) 111.
[26] (a) M. Meza, M. Mediavilla, D. Pineda, P. Baricelli, A. Pardey, Rev. Soc. Venez. Catal. 8 (1994) 29;
(b) M.A. Fernández, M. Meza, M. Mediavilla, C. Longo, S.A. Moya, F. López, P. Baricelli, A.J. Pardey, Anal. Quím. Int. Ed. 94 (1998) 127;
(c) A.J. Pardey, M.A. Moreno, M.C. Ortega, B. Mendez, A.B. Rivas, S.A. Moya, D. Villagra, M. Lutz, J. Chil. Chem. Soc. 48 (2003) 19;
(d) A.J. Pardey, M.A. Moreno, M. Lutz, M. Haukka, R. Atencio, Acta Cryst. E 62 (2006) m838;
(e) C. Linares, M. Mediavilla, A.J. Pardey, C. Longo, P. Baricelli, S.A. Moya, Bol. Soc. Chil. Quim. 43 (1998) 55.